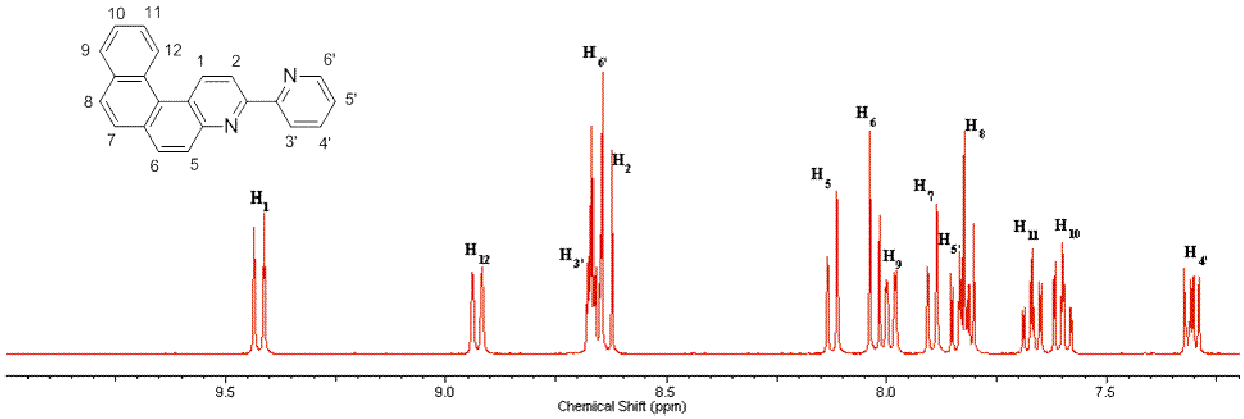

Figure S1. ^{1}H NMR of ligand **1b** in CD_2Cl_2 (400 MHz).

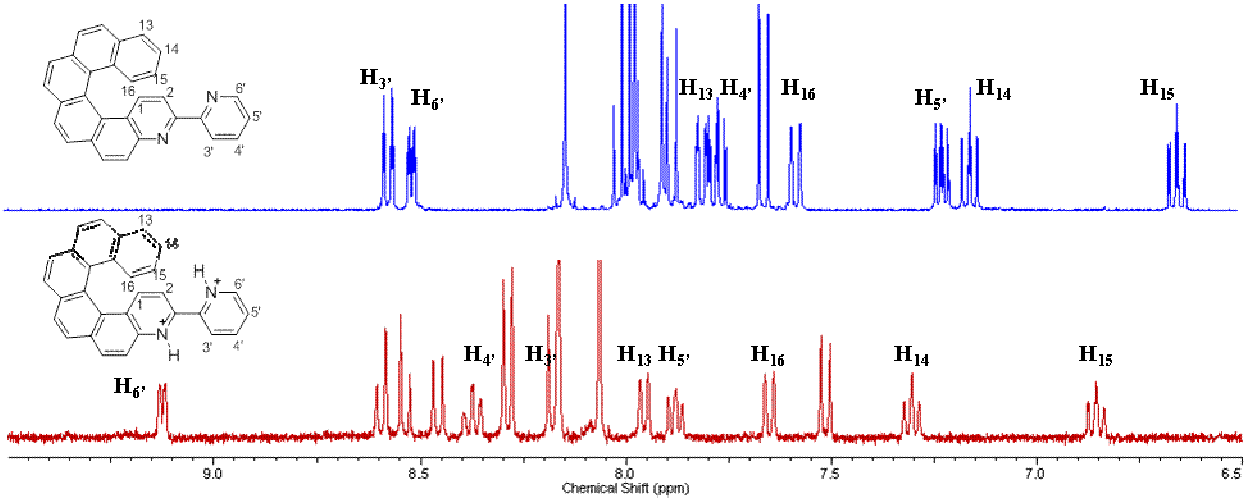

Figure S2. ^{1}H NMR of ligand **1a** and [**1a**,$2H^+$][$2BF_4^-$] in CD_2Cl_2 (400 MHz).

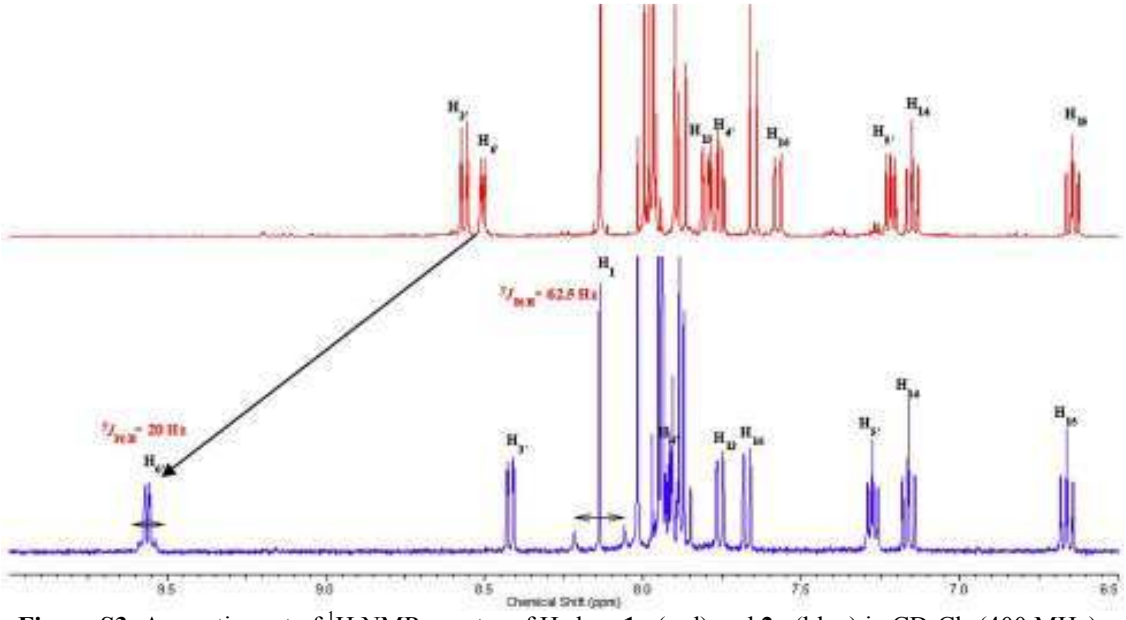

Figure S3: Aromatic part of ^{1}H NMR spectra of H_4-bpy **1a** (red) and **2a** (blue) in CD_2Cl_2 (400 MHz).

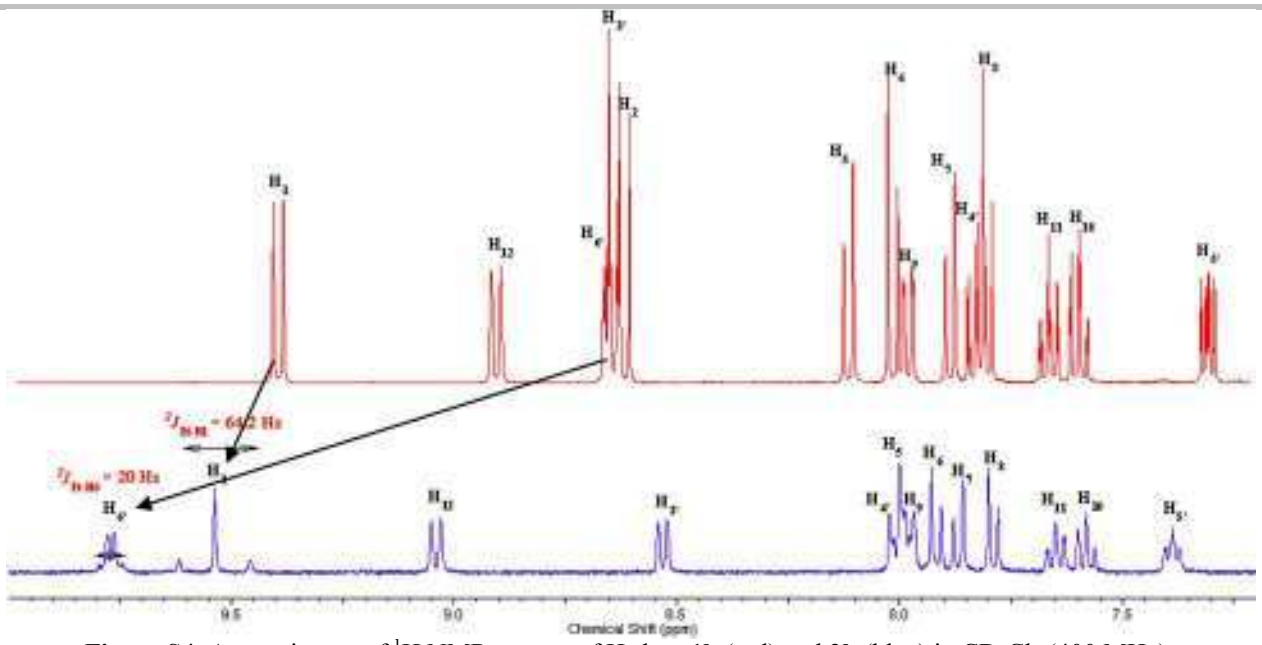

Figure S4: Aromatic part of ^{1}H NMR spectra of H_4-bpy **1b** (red) and **2b** (blue) in CD_2Cl_2 (400 MHz).

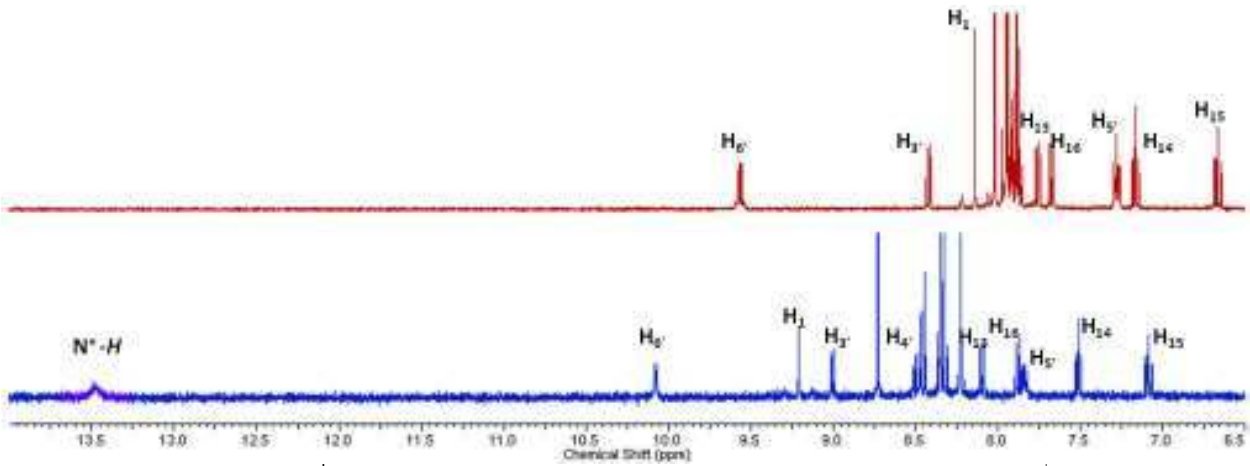

Figure S5: Aromatic region ^{1}H NMR spectra of protonated "roll-over" cyclometalated [**2a**,H^+][BF_4^-] complex (blue) in CD_2Cl_2 (400 MHz), compared to **2a** (red).

HPLC separations

Analytical chiral HPLC separation for compound **1a**

• The sample is dissolved in a mixture ethanol/chloroform (1/1), injected on the chiral columns, and detected with an UV detector at 254 nm and a polarimeter. The flow-rate is 1 ml/min.

Column	Mobile Phase	t1	k1	t2	k2	α	Rs
Chiralpak IC	Hexane/ethanol/chloroform 90/5/5	6.33 (+)	1.11	7.98 (-)	1.66	1.50	2.76

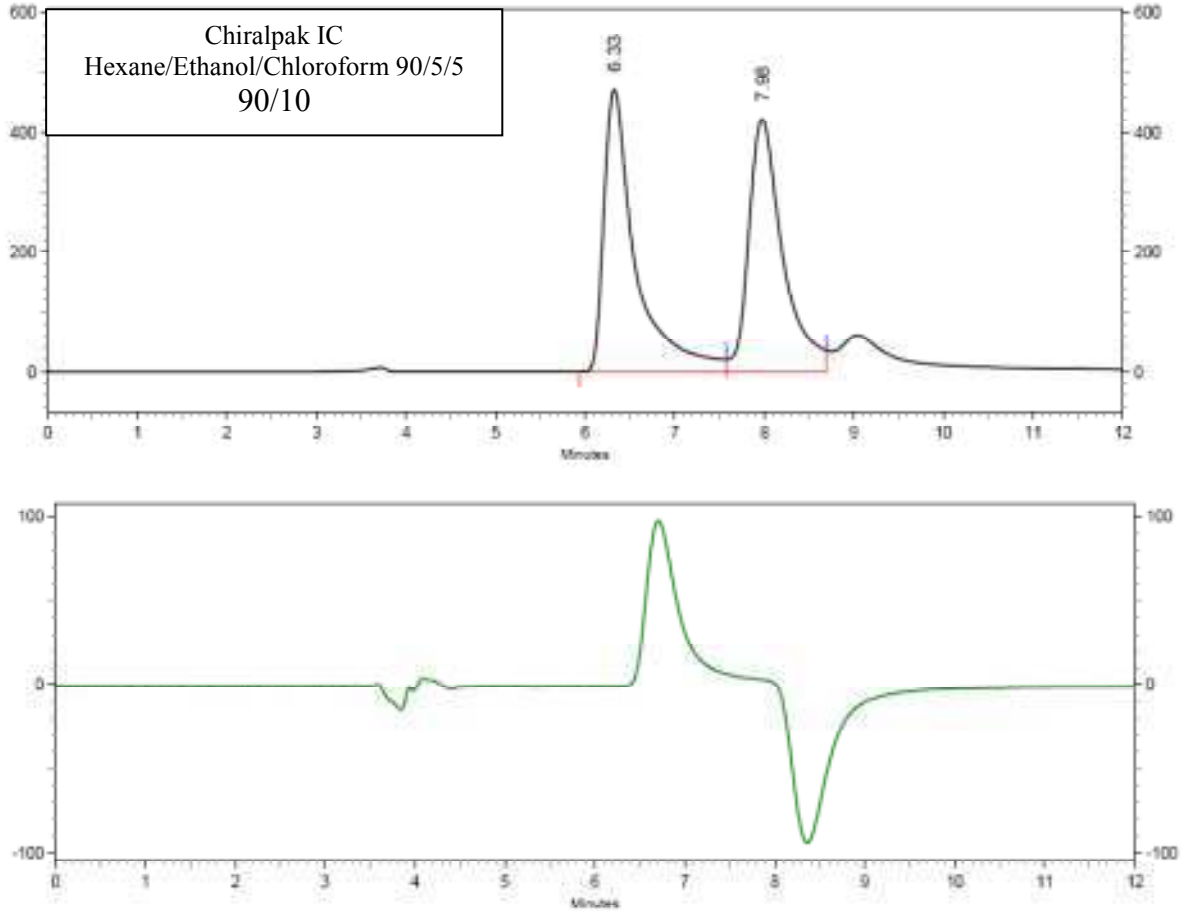

1: 254 nm, 4 nm

Results

Retention Time	Area	Area %	Capacity factor	Relative RT	Resolution (USP)
6.33	46092707	51.01	1.11	1.00	0.00
7.98	44259812	48.99	1.66	1.50	2.76
Totals	90352519	100.00			

Semi-preparative separation for compound **1a**:

- Sample preparation: About 600 mg of compound **1a** are dissolved in 280 ml of chloroform/hexane 1/1.
- Chromatographic conditions: Chiralpak IC (250 x 10 mm), thermostated at 30 °C, hexane/ethanol/chloroform 90/5/5 as mobile phase, flow-rate = 5 ml/min, UV detection at 385 nm.
- Injection: 350 times 800 µl, every 12 minutes.
- Collection: the first eluted enantiomer is collected between 6 and 7.7 minutes and the second one between 8.2 and 10 minutes.
- First fraction: 273 mg of the first eluted ((+)-enantiomer) with *ee* > 99%
- Second fraction: 257 mg of the second eluted ((-)-enantiomer) with *ee* > 99%
- Chromatograms of the collected enantiomers:

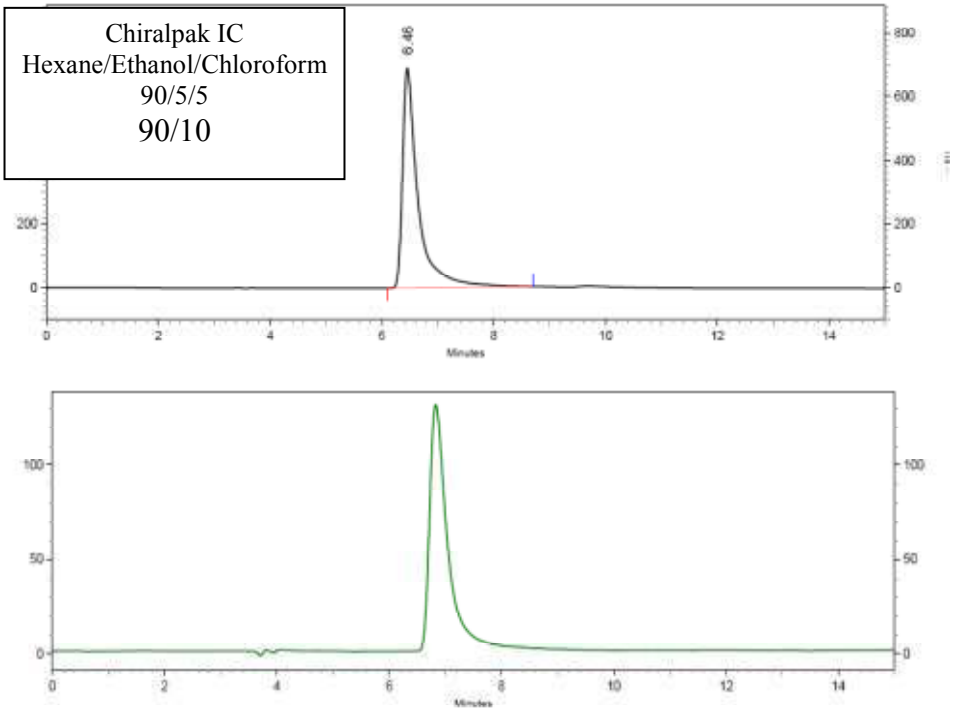

1: 254 nm, 4 nm
Results

Retention Time	Area	Area %	Capacity factor	Relative RT	Resolution (USP)
6.46	53587461	100.00	1.15	1.00	0.00
Totals	53587461	100.00			

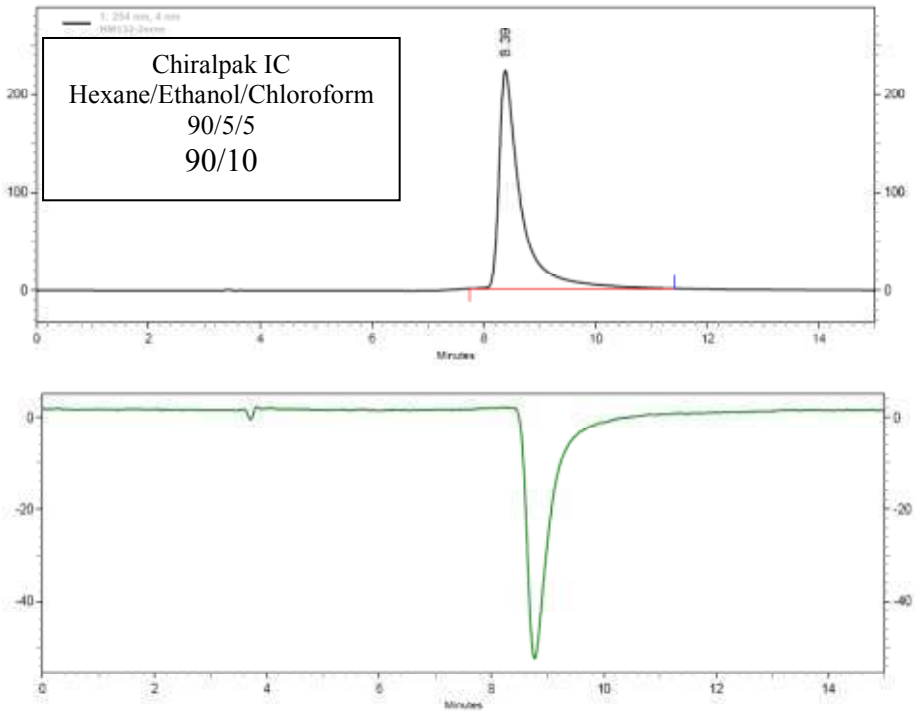

1: 254 nm, 4 nm
Results

Retention Time	Area	Area %	Capacity factor	Relative RT	Resolution (USP)
8.39	23652673	100.00	1.80	0.00	0.00
Totals	23652673	100.00			

Analytical chiral HPLC separation for compound **1a**

• The sample is dissolved in chloroform, injected on the chiral columns, and detected with an UV detector at 254 nm and CD 254nm. The flow-rate is 1 mL/min.

Column	Mobile Phase	t1	k1	t2	k2	α	Rs
Chiralpak IA	Hexane / 2-PrOH with 0.1% triethylamine / chloroform (7/1/2)	4.52 (+)	0.51	4.87 (-)	0.62	1.21	0.86
Chiralpak IB		4.31	0.44			1	0
Chiralpak IC		5.17 (-)	0.72	8.05 (+)	1.68	2.33	4.95
Chiralpak ID		5.35 (+)	0.78	8.16 (-)	1.72	2.19	6.43
Chiralpak IE		10.40 (-)	2.47	14.06 (+)	3.69	1.49	3.87
Chiralpak IF		5.59 (+)	0.86	6.13 (-)	1.04	1.21	1.30

Experimental optical rotation values

P-(+)-**1a**: $[\alpha]_D^{23}$ = +2955, $[\phi]_D^{23}$ = +12000 ((±5%), CH_2Cl_2, 6.5 10^{-5} mol·L^{-1})

M-(-)-**1a**: $[\alpha]_D^{23}$ = -2951, $[\phi]_D^{23}$ = -11995 ((±5%), CH_2Cl_2, 6 10^{-5} mol·L^{-1})

P-[**1a**,$2H^+$][$2BF_4^-$]: $[\alpha]_D^{23}$ = +1700, $[\phi]_D^{23}$ = +10000 ((±5%), in CH_2Cl_2, 1.7 10^{-4} M)

M-[**1a**,$2H^+$][$2BF_4^-$]: $[\alpha]_D^{23}$ = -1660, $[\phi]_D^{23}$ = -9663 ((±5%), in CH_2Cl_2, 1.7 10^{-4} M)

P-(+)-**2a**: $[\alpha]_D^{23}$ = +2700, $[\phi]_D^{23}$ = +18730 ((±5%), CH_2Cl_2, 7 10^{-5} mol·L^{-1})

M-(-)-**2a**: $[\alpha]_D^{23}$ = -2695, $[\phi]_D^{23}$ = -18700 ((±5%), CH_2Cl_2, 6 10^{-5} mol·L^{-1})

P-[**2a**,H^+][BF_4^-]: $[\alpha]_D^{23}$ = +1170, $[\phi]_D^{23}$ = +9145 ((±5%), in CH_2Cl_2, 1.5 10^{-5} M)

M-[**2a**,H^+][BF_4^-]: $[\alpha]_D^{23}$ = -1188, $[\phi]_D^{23}$ = -9281 ((±5%), in CH_2Cl_2, 10^{-4} M)

Experimental UV-vis and circular dichroism spectra

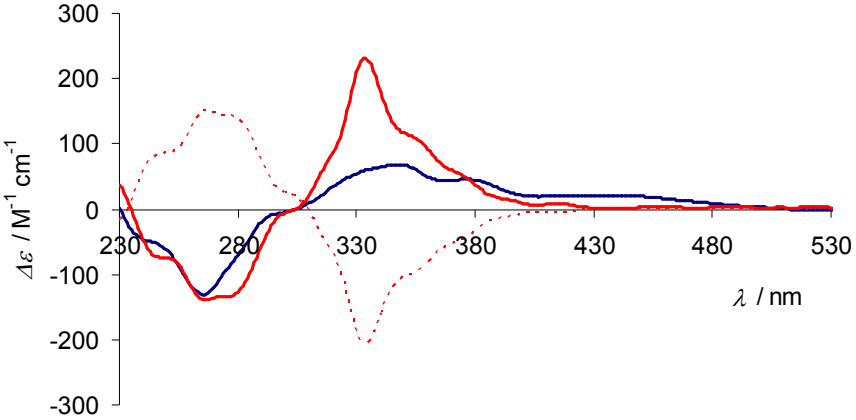

Figure S6. ECD spectra of *P*-**1a** (red plain lines), *M*-**1a** (red dashed lines) and *P*-[**1a**,$2H^+$][$2BF_4^-$] (blue plain lines) in CH_2Cl_2.

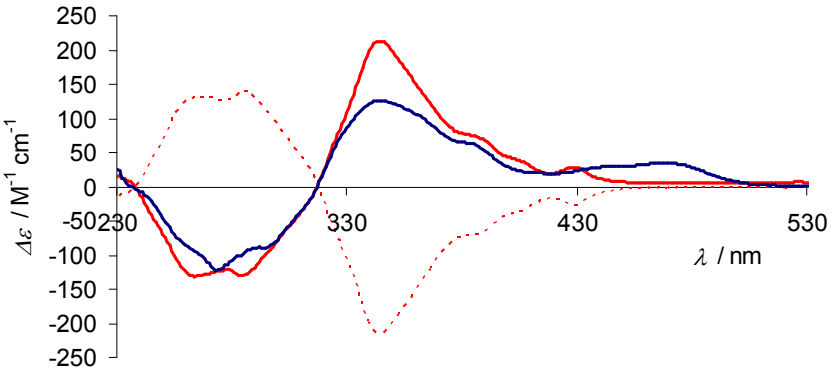

Figure S7. ECD spectra of *P*-**2a** (red plain lines), *M*-**2a** (red dashed lines) and *P*-[**2a**,H^+][BF_4^-] (blue plain lines) in CH_2Cl_2.

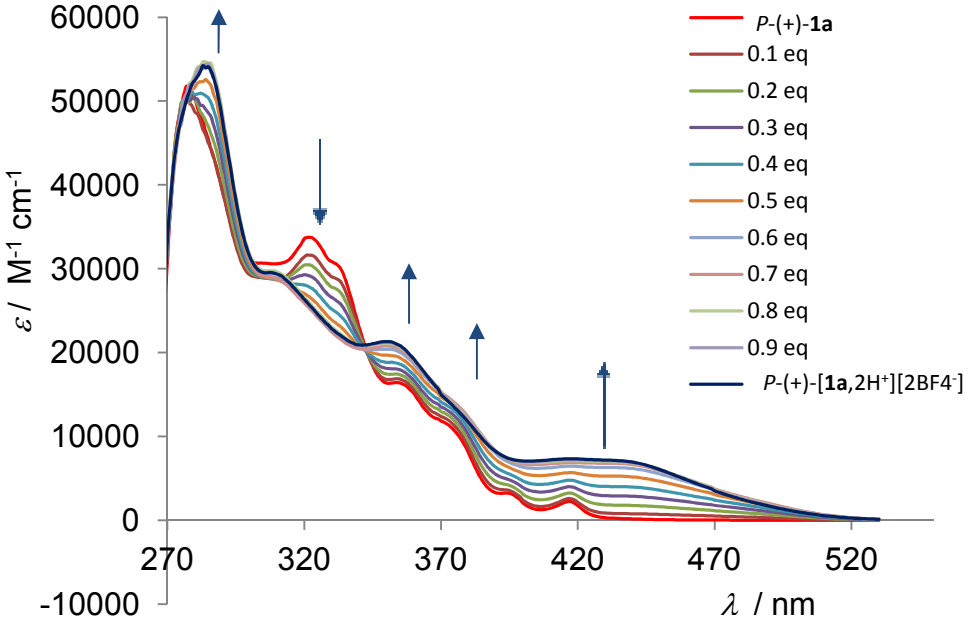

Figure S8. UV-Vis titration in CH_2Cl_2 of **1a** upon additions of $[H_2O.HBF_4]_2[18C6]$.

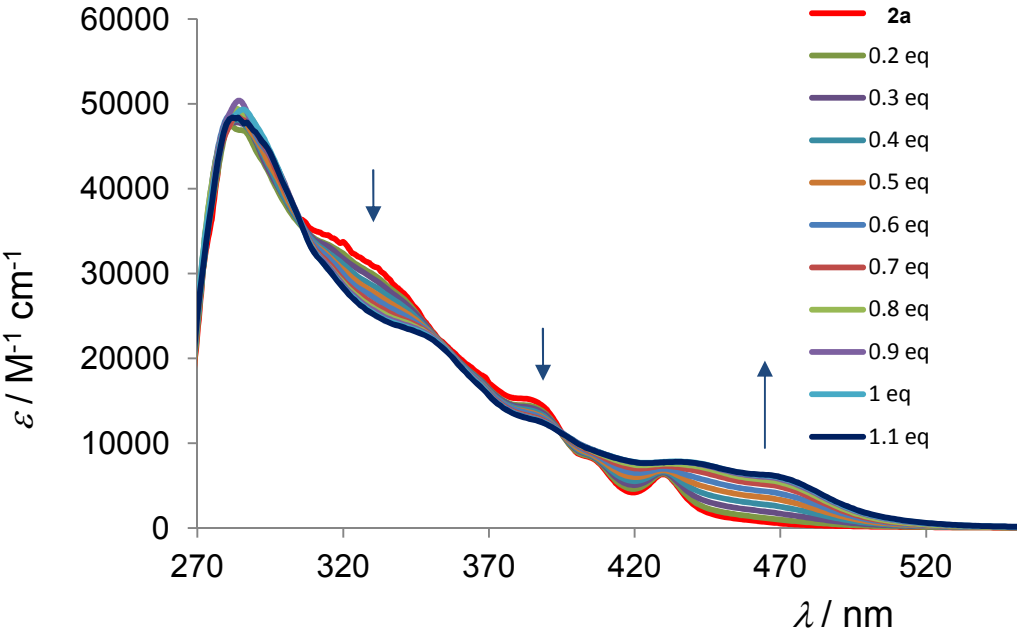

Figure S9. UV-Vis titration in CH_2Cl_2 of **2a** upon additions of $[H_2O.HBF_4]_2[18C6]$.

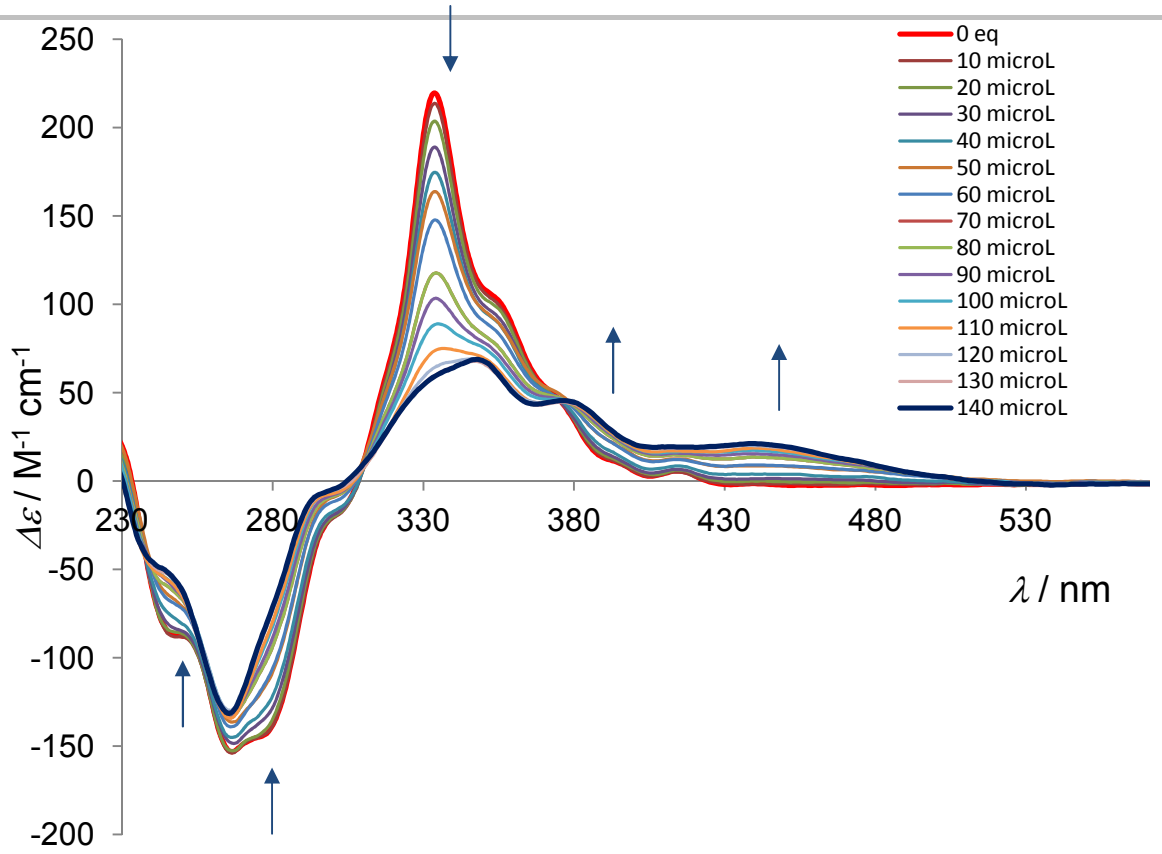

Figure S10. CD titration in CH_2Cl_2 of *P*-**1a** upon additions of $[H_2O.HBF_4]_2[18C6]$.

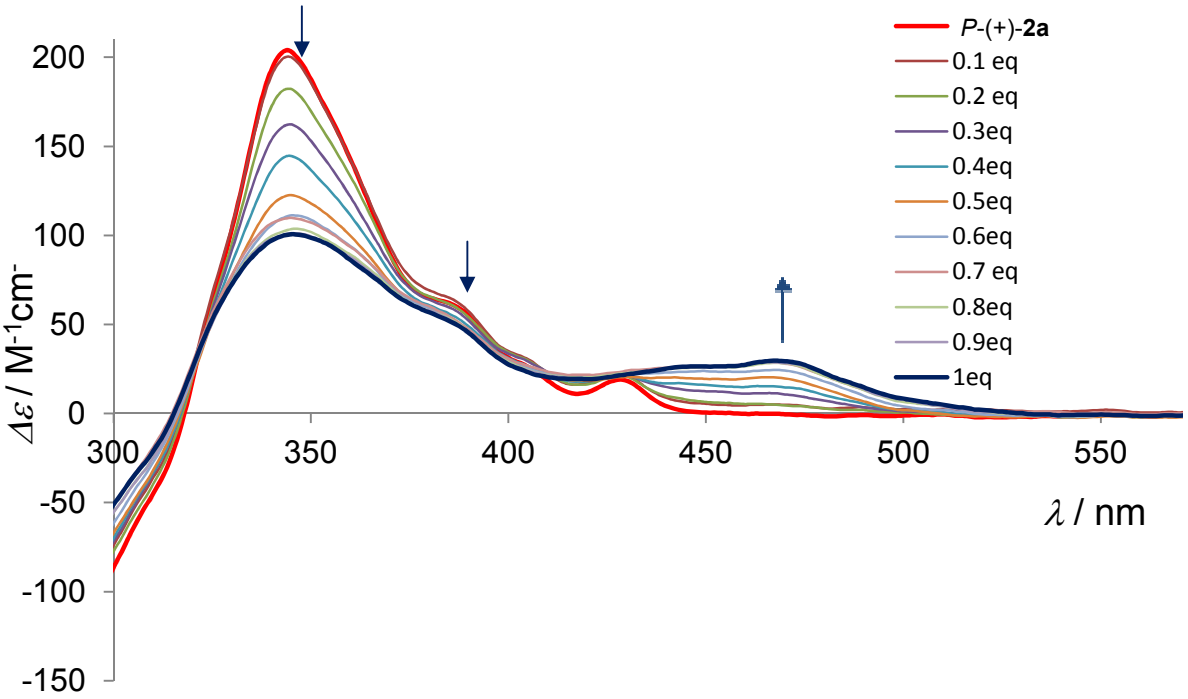

Figure S11. CD titration in CH_2Cl_2 of *P*-**2a** upon additions of $[H_2O.HBF_4]_2[18C6]$.

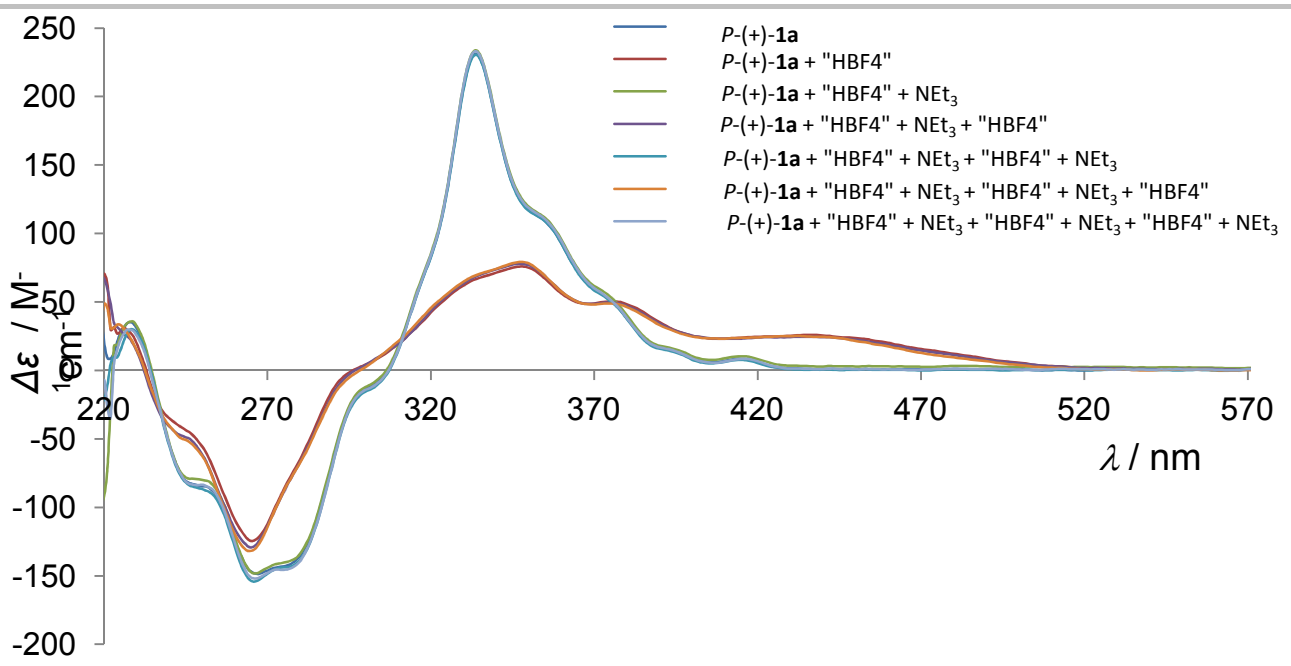

Figure S12. Acid-base ECD switching of complex *P*-(+)-**1a** upon successive additions of $[H_2O.HBF_4]_2[18C6]$ and of Et_3N.

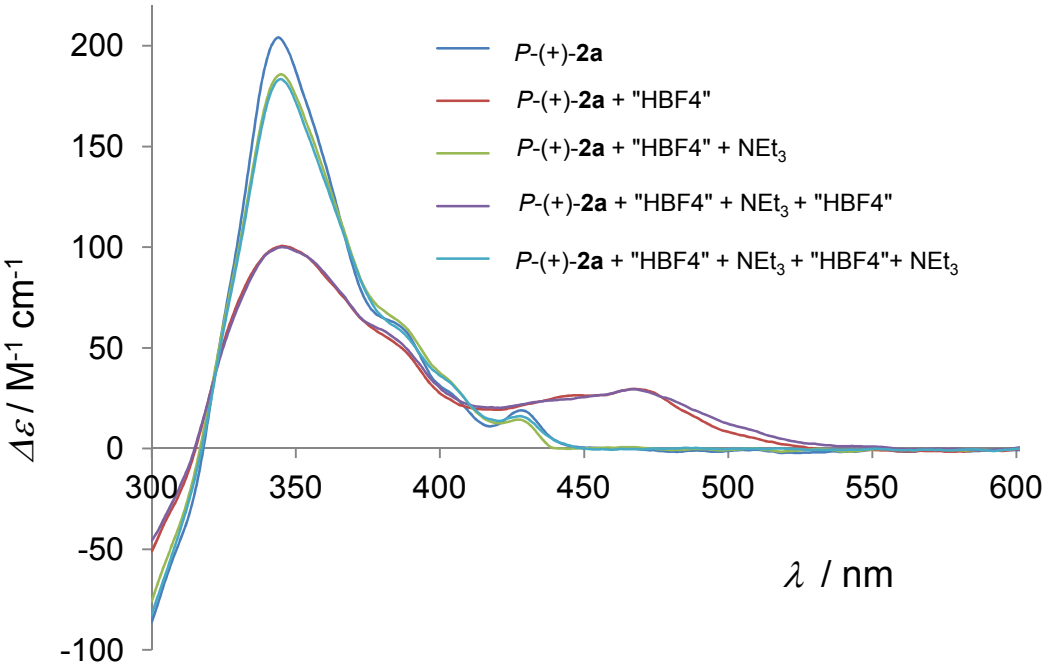

Figure S13. Acid-base ECD switching of complex *P*-(+)-**2a** upon successive additions of $[H_2O.HBF_4]_2[18C6]$ and of NEt_3 in acetone.

X-Ray diffraction results

Figure S14. X-ray structure of ligand **1b** and of complex (H_4-bpy)Pt(PPh_3)Cl **3b**

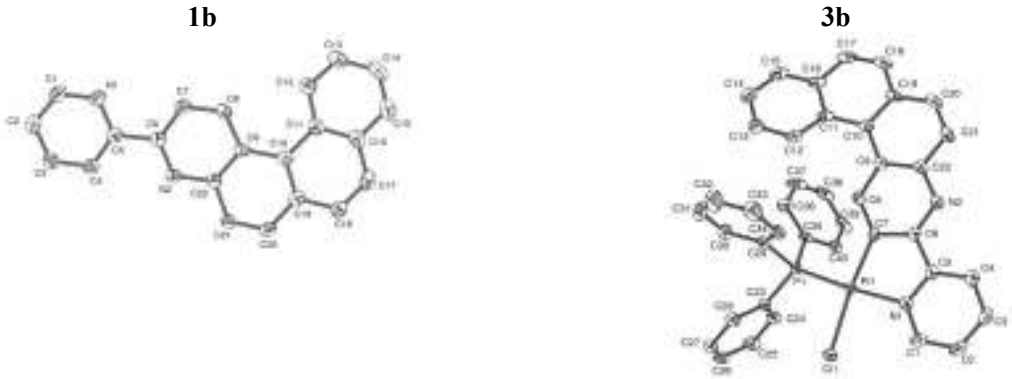

Figure S15. ORTEP diagrams of proligand **1b** and complex 3b with ellipsoids at 50% probability.

Table S1 Selected Bond Distances (Å) and Angles (deg) in **3b** in comparison with the reference bpyPtClPPh$_3$ and the free proligand **1b**

	3b	**bpyPtClPPh$_3$**[6]	**1b**
Pt-Cl	2.386	2.380	
Pt-P	2.228	2.223	
Pt-N$_1$	2.108	2.097	
Pt-C$_7$	2.002	2.008	
N$_1$-C$_5$	1.355	1.349	1.314
C$_5$-C$_6$	1.466	1.463	1.481
C$_6$-C$_7$	1.423	1.416	1.402
Cl-Pt-P	91.97°	92.75°	
Cl-Pt-N$_1$	92.2°	90.77°	
Cl-Pt-C$_7$	173.02°	170.97°	
P-Pt-N$_1$	175.83°	176.24°	
P-Pt-C$_7$	95.01°	95.80°	
N$_1$-Pt-C$_7$	80.81°	80.77°	
Helicity	28.8°		25.31°

Table S2. X-ray crystallographic data

	1b	**3b**
Empirical Formula	$C_{22}H_{14}N_2$	$C_{40}H_{28}ClN_2PPt$
CCDC number	927001	934302
Formula Weight	306.35	798.15
Temperature (K)	100(2)	120(2)
Wavelenght (Å)	0.71073	0.71073
Crystal system	Orthorhombic	Triclinic
Space Group	$P2_12_12_1$	P-1
a (Å)	4.7136(2)	9.3961(2)
b (Å)	13.0891(9)	10.3378(2)
c (Å)	23.6221(10)	15.9069(3)
α (Å)	90	91.674(2)
β (Å)	90	103.563(2)
γ (Å)	90	90.529(2)
Volume (Å^3)	1457.41(13)	1501.18(5)
Z	4	2
Color	yellow	yellow
$\rho_{calculated}$ (g.cm^{-3})	1.396	1.766
Absorption coefficient (mm^{-1})	0.083	4.850
F(000)	640.0	784
Crystal size (mm)	0.342*0.124*0.118	0.283*0.236*0.149
θ range for data collection (º)	3.02 to 26.99	2.64 to 27.0
Tmin	0.988	0.264
Tmax	0.990	0.485
Limiting indices	$-5 \le h \le 6$ $-16 \le k \le 14$ $-30 \le l \le 28$	$-12 \le h \le 12$ $-13 \le k \le 13$ $-20 \le l \le 20$
Data completeness	99.7% (θ = 26.99º)	99.9% (θ = 27.00º)
Reflections collected	10719	19078
Reflections unique	3149 [R(int) = 0.0731]	6528 [R(int) = 0.0302]
Data / restraints / parameters	3149 / 0 / 217	6528 / 0 / 406
Goodness-of-fit on F^2	0.807	0.989
Final R indices [I>2 σ (I)]	R1 = 0.0439, wR2 = 0.0765	R1 = 0.0202, wR2 = 0.0460
R indices (all data)	R1 = 0.0902, wR2 = 0.0857	R1 = 0.0238, wR2 = 0.0466
Largest diff peak and hole (e Å^{-3})	0.195 and -0.194	1.459 and -0.956

Non-polarised luminescence measurements

Instrumentation

Absorption spectra were measured on a Biotek Instruments XS spectrometer, using quartz cuvettes of 1 cm path length. Steady-state luminescence spectra were measured using a Jobin Yvon FluoroMax-2 spectrofluorimeter, fitted with a red-sensitive Hamamatsu R928 photomultiplier tube; the spectra shown are corrected for the wavelength dependence of the detector, and the quoted emission maxima refer to the values after correction. Samples for emission measurements were contained within quartz cuvettes of 1 cm path length modified with appropriate glassware to allow connection to a high-vacuum line. Degassing was achieved via a minimum of three freeze-pump-thaw cycles whilst connected to the vacuum manifold; final vapour pressure at 77 K was $< 5 \times 10^{-2}$mbar, as monitored using a Pirani gauge. Luminescence quantum yields were determined using $[Ru(bpy)_3]Cl_2$ in degassed aqueous solution as the standard ($\Phi_{lum} = 0.042$); estimated uncertainty in Φ_{lum} is ± 20% or better, except where indicated otherwise.Luminescence lifetimes < 10 μs were measured by time-correlated single-photon counting, following excitation at 374.0 nm with an EPL-375 pulsed-diode laser. The emitted light was detected at 90° using a Peltier-cooled R928 PMT after passage through a monochromator. Lifetimes > 10 μs were measured using the same detector in multichannel scaling mode following excitation with a microsecond pulsed xenon lamp. The estimated uncertainty in the quoted lifetimes is ± 10% or better.

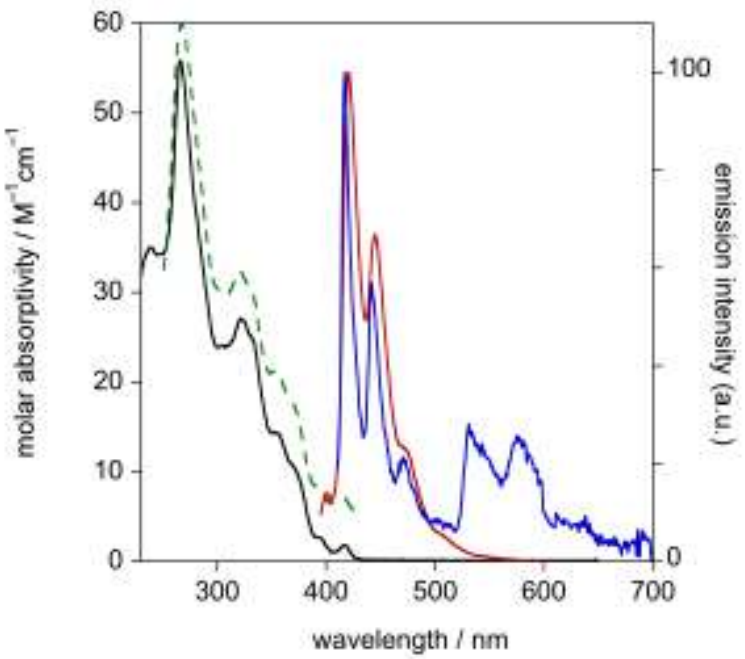

Figure S16. Spectra of **1a**: absorption (black line), fluorescence emission (red line) and fluorescence excitation (green dashed line) spectra at room temperature in CH_2Cl_2; emission spectrum in diethyl ether / isopentane / ethanol (2:2:1 v/v) at 77 K (blue line).

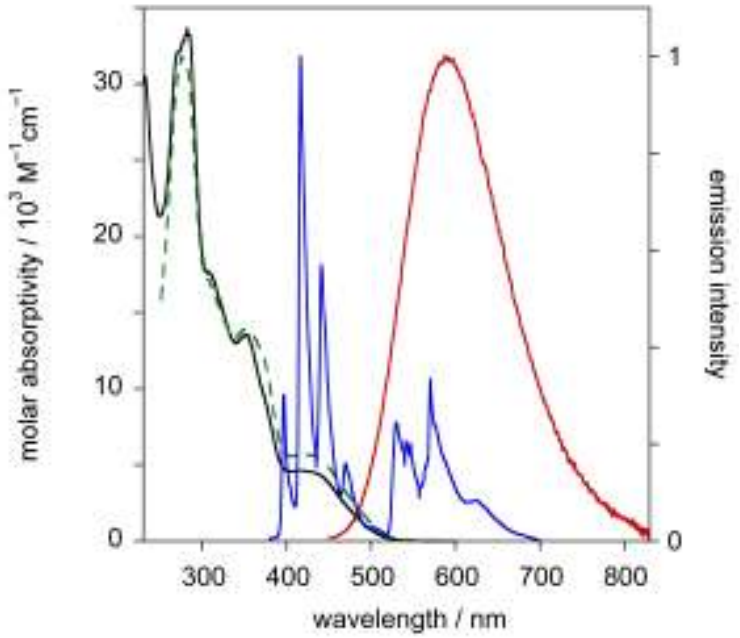

Figure S17. Spectra of [**1a**,$2H^+$][$2BF_4^-$]: absorption (black line), fluorescence emission (red line) and fluorescence excitation (green dashed line) spectra at room temperature in CH_2Cl_2; emission spectrum in diethyl ether / isopentane / ethanol (2:2:1 v/v) at 77 K (blue line).

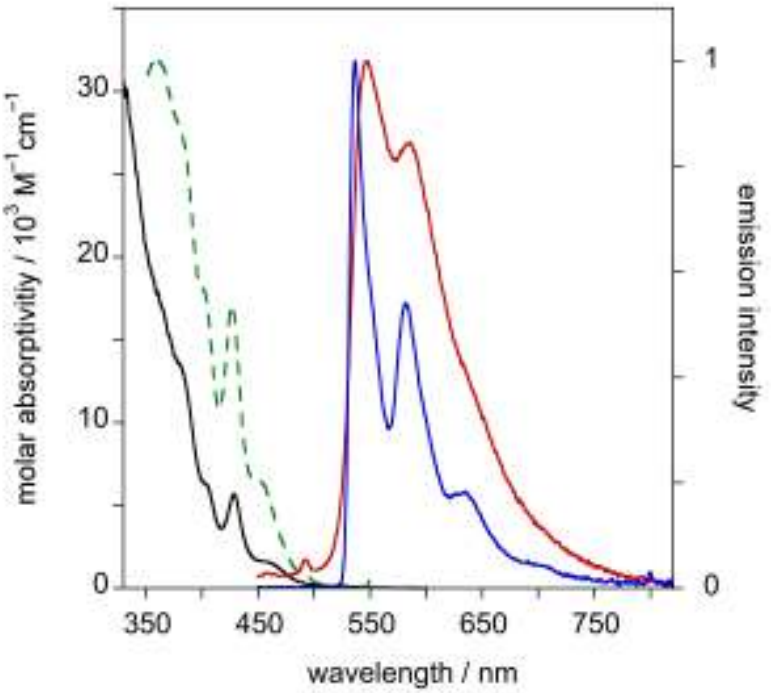

Figure S18. Spectra of **2a**: absorption (black line), emission (red line) and excitation (dashed green line) spectra in acetone at room temperature; emission spectrum in diethyl ether / isopentane / ethanol (2:2:1 v/v) at 77 K (blue line).

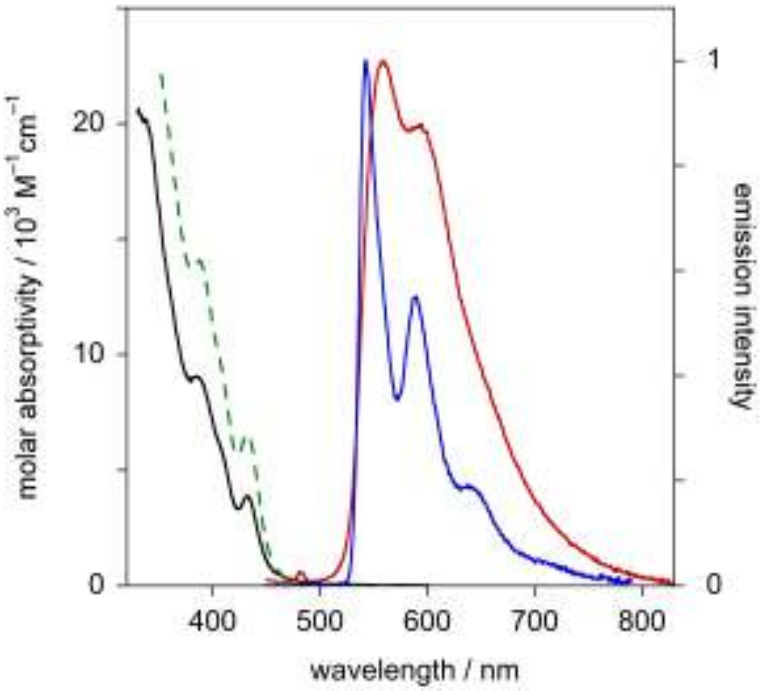

Figure S19. Spectra of [**2a**,H^+][BF_4^-]: absorption (black line), emission (red line) and excitation (dashed green line) spectra in acetone at room temperature; emission spectrum in diethyl ether / isopentane / ethanol (2:2:1 v/v) at 77 K (blue line).

Table S3 Summary of absorption and non-polarised photoluminescence data.

Compound	**Absorption** λ_{max} **/ nm (**ε **/** $M^{-1}cm^{-1}$**)**	**Emission** λ_{max} **/ nm**	**Φ**[(c)]	**τ / ns**[(c)]	**Emission 77K**[(d)]	
					λ_{max} **/ nm**	**τ / ns**
1a[(a)]	240 (35000), 266 (55800), 322 (27000), 353 (14400), 372 (10200), 393 (2630), 417 (1800)	421, 445, 473sh	0.084	6.6 ns	F = 417, 442, 471	9.0 ns
					P = 531, 577, 624	1.3 s
[**1a**,$2H^+$][$2BF_4^-$][(a)]	282 (33700), 308sh (17600), 351 (13600), 418 (4630)	590	0.082	5.4 ns	F = 396, 416, 441, 470[(e)]	9.8 ns
					P = 530, 577, 621[(e)]	1.4 s
2a[(b)]	379sh (13600), 402sh (6340), 429 (5680), 458 (1590)	547, 585	0.0038	18 μs	536, 582, 635	890μs
[**2a**,H^+][BF_4^-] [(b)]	385 (9060), 432 (3890)	555, 590	0.027	120μs	542, 589, 640[(e)]	720μs

(a) In dichloromethane at 298 ± 3K, except where indicated otherwise. *(b)* In acetone at 298 ± 3K except where indicated otherwise (note that absorption maxima < 330 nm are not measurable in acetone, due to the solvent absorption). *(c)* In degassed solution. (*d*) Data at 77 K recorded in diethyl ether / isopentane / ethanol (2:2:1 v/v). *(e)* Note that at 77 K the equilibrium $B+H^+ \rightleftarrows BH^+$ is frozen.

CPL measurements

The circularly polarized luminescence (CPL) and total luminescence spectra were recorded on an instrument described previously,[1] operating in a differential photon-counting mode. The light source for excitation was a continuous wave 1000 W xenon arc lamp from a Spex Fluorolog-2 spectrofluorimeter, equipped with excitation and emission monochromators with dispersion of 4 nm/mm (SPEX, 1681B). To prevent artifacts associated with the presence of linear polarization in the emission,[2] a high quality linear polarizer was placed in the sample compartment, and aligned so that the excitation beam was linearly polarized in the direction of emission detection (z-axis). The key feature of this geometry is that it ensures that the molecules that have been excited and that are subsequently emitting are isotropically distributed in the plane (x,y) perpendicular to the direction of emission detection. The optical system detection consisted of a focusing lens, long pass filter, and 0.22 m monochromator. The emitted light was detected by a cooled EMI-9558B photomultiplier tube operating in photo-counting mode. All measurements were performed with quartz cuvettes with a path length of 1.0 cm.

References

[1] Brunet, E.; Jiménez, L.; de Victoria-Rodriguez, M.; Luu, V.; Muller, G.; Juanes, O.; Rodríguez-Ubis, J.C. *Microporous and Mesoporous Mater.*, **2013**, *169*, 222, and references therein.
[2] Dekkers, H. P. J. M.; Moraal, P. F.; Timper, J. M.; Riehl, J. P. *Appl. Spectrosc.* **1985**, *39*, 818.

Computational Details

Optimized geometries of *P*-**1a**, *P*-[**1a**,2H$^+$], *P*-**2a**, and *P*-[**2a**,H$^+$] were obtained using the Turbomole program[1] version 6.5, with the Becke-Perdew (BP) density functional[2–4] and a split-valence basis SV(P),[5] which includes polarization functions for non-hydrogen atoms. A 60 electron effective-core potential (ECP) was employed for platinum.[6] The basis set / ECP definition is available at the EMSL basis set exchange.[7,8]

The sodium-D line (λ = 589.3 nm) optical rotations (ORs) and electronic circular dichroism (ECD) spectra were calculated with the BHLYP[9,10] functional and the same basis set and ECP as aforementioned using the Turbomole TDDFT module. All CD calculations covered the 100 lowest singlet excited states (S1 to S100) for each system. The simulated spectra shown are the sums of Gaussian functions centered at the vertical excitation energies and scaled using the calculated rotatory strengths, with a parameter of σ = 0.2 eV applied for the root mean square width. Electronic emission spectra via S_1 and T_1 excited-states geometry optimizations were obtained using the Gaussian 09 program[11] with BHLYP/SV(P). In the case of triplet states calculations, the Tamm-Dancoff approximation (TDA)[12–17] was applied, as full TDDFT results were found to be unreliable.

Some benchmark CD computations employed a functional with range-separated exchange, LC-wPBE,[18–20] and were carried out using the Gaussian 09 program. CD calculations were additionally carried out using a range-separated exchange functional based on LC-PBE0[21,22] optimally tuned for a helicene, using a developers version of NWChem[23] with the same basis set. The motivation and background of optimal tuning is well established in the literature.[24–38] An optimal range-separation parameter γ (0.143 a_0^{-1}) was taken from previous work by the authors on optical rotation of helicene derivatives.[30] There is an appearance of new low-energy CD bands upon protonation of **1a** and **2a** which are shown below to have a significantly increased charge-transfer character compared to the lowest-energy excitations of the non-protonated species. The excellent agreement of BHLYP with the LC calculations establishes that BHLYP, which reproduces the experimental spectra well, does not suffer from a charge-transfer breakdown in the TDDFT calculations.

Solvent effects (dichloromethane, DCM, ε = 8.9; acetone, ε = 20.7) were included in the calculations in order to improve the correspondence with experimental results. This was found to be particularly important in the case of the protonated ligand species, for which gas-phase TDDFT results were found to be clearly deficient.[39] The conductor-like screening model (COSMO)[40–42] and polarizable continuum model (PCM)[42–45] with default parameters were employed in Turbomole and Gaussian, respectively.

Counter-ion (BF_4^-) effects were considered for both protonated species, *P*-[**1a**,2H$^+$] and *P*-[**2a**,H$^+$], since the presence of a counter-ion may affect the calculated chiroptical properties. For this purpose, the BF_4^- was placed near the protonated nitrogen, and the geometry was optimized with use of a continuum solvent model. The counter-ions had the strongest effect on the protonated **1a** ligand, which additionally reveals high conformational flexibility. The reader is referred to Table S4 for preliminary OR data obtained for both protonated species in the presence of counter-ions, showing that coordination of the systems by solvent as well as the counter-ion(s) is likely responsible for the much smaller experimentally determined ORs in comparison to the calculations with just the continuum solvent model. Figure S22 shows the corresponding CD spectra, indicating an improvement for *P*-[**1a**,2H$^+$] and relatively minor, but noticeable, changes for *P*-[**2a**,H$^+$]. In a follow-up study we will investigate explicit solvent effects and counter-ion effects in detail using *ab-initio* molecular dynamics (aiMD). Due to the very high computational effort of aiMD-based

averaging of optical properties and spectra, and due to the fact that the CD and CPL spectra and not the ORs are the main focus of the present report, such calculations are beyond the scope of this Manuscript.

Table S4. Calculated optical rotations for cycloplatinated complexes *P*-**2a** and *P*-[**2a**,H^+], and the pristine ligand species *P*-**1a** and *P*-[**1a**,$2H^+$], along with experimental data. [a]

System	# / ΔE	∠ N-C-C'-N'	**Calc. BHLYP/SV(P)**		Expt.	
			$[\alpha]_D$	$[\phi]_D$	$[\alpha]_D$	$[\phi]_D$
1a	---	179.7	3487	14176	2955	12000
[**1a**,$2H^+$] [b]	1 / 0.00	-150.0	8835	36092	1700	10000
	2 / 0.35	151.0	9147	37367		
	3 / 0.94	-178.2	11984	48953		
2a	---	---	2789	19345	2700	18730
[**2a**,H^+] [b]	---	---	3486	24217	1170	9145

[a] Dichloromethane (DCM, $\varepsilon = 8.9$) solution. '#' numbers different conformers. BP/SV(P) relative energy ΔE given in kcal/mol, dihedral angle N-C-C'-N' (compare Figure S20) in degree, specific rotations and molar rotations in degree/(dm g/cm^{-3}) and degree cm^2/dmol, respectively. [b] Calculations performed with an optimized structure of [**1a**,$2H^+$][$2BF_4^-$] resulted in strongly decreased OR values: 3687 and 21463 for specific and molar rotation, respectively. Similar calculations for two different optimized [**2a**,H^+][BF_4^-] structures yielded 2886/2843 and 22553/22222 for specific and molar rotation, respectively. Compare Figure S21.

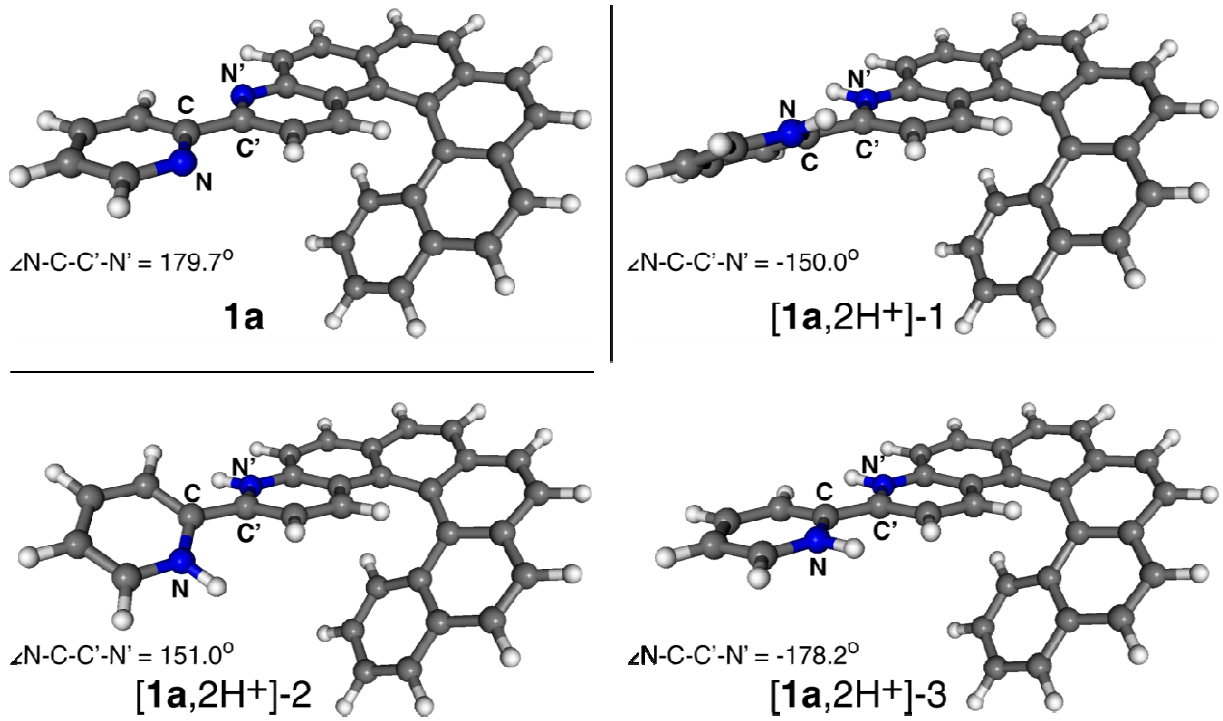

Figure S20. Selected low-energy optimized structures of ligand species *P*-**1a** and *P*-[**1a**,2H$^+$]. BP/SV(P) DCM calculations.

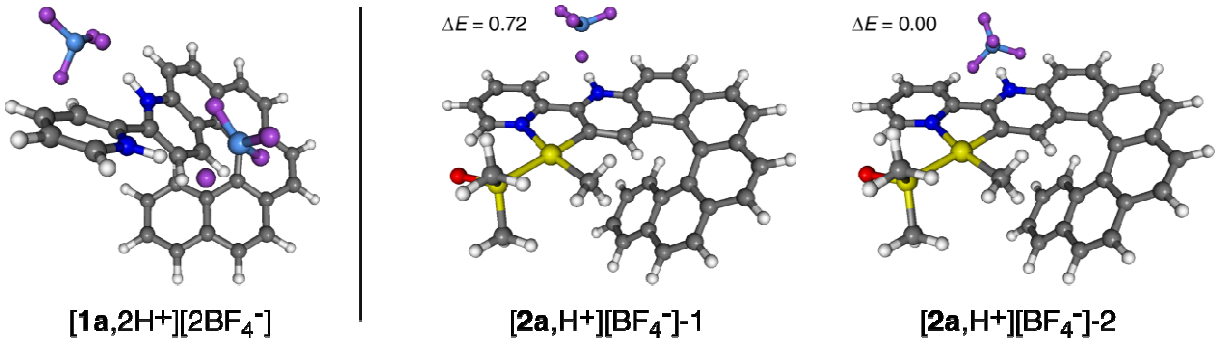

Figure S21. Optimized structures of protonated species. BP/SV(P) DCM calculations. Relative energies, Δ*E*, given in kcal/mol.

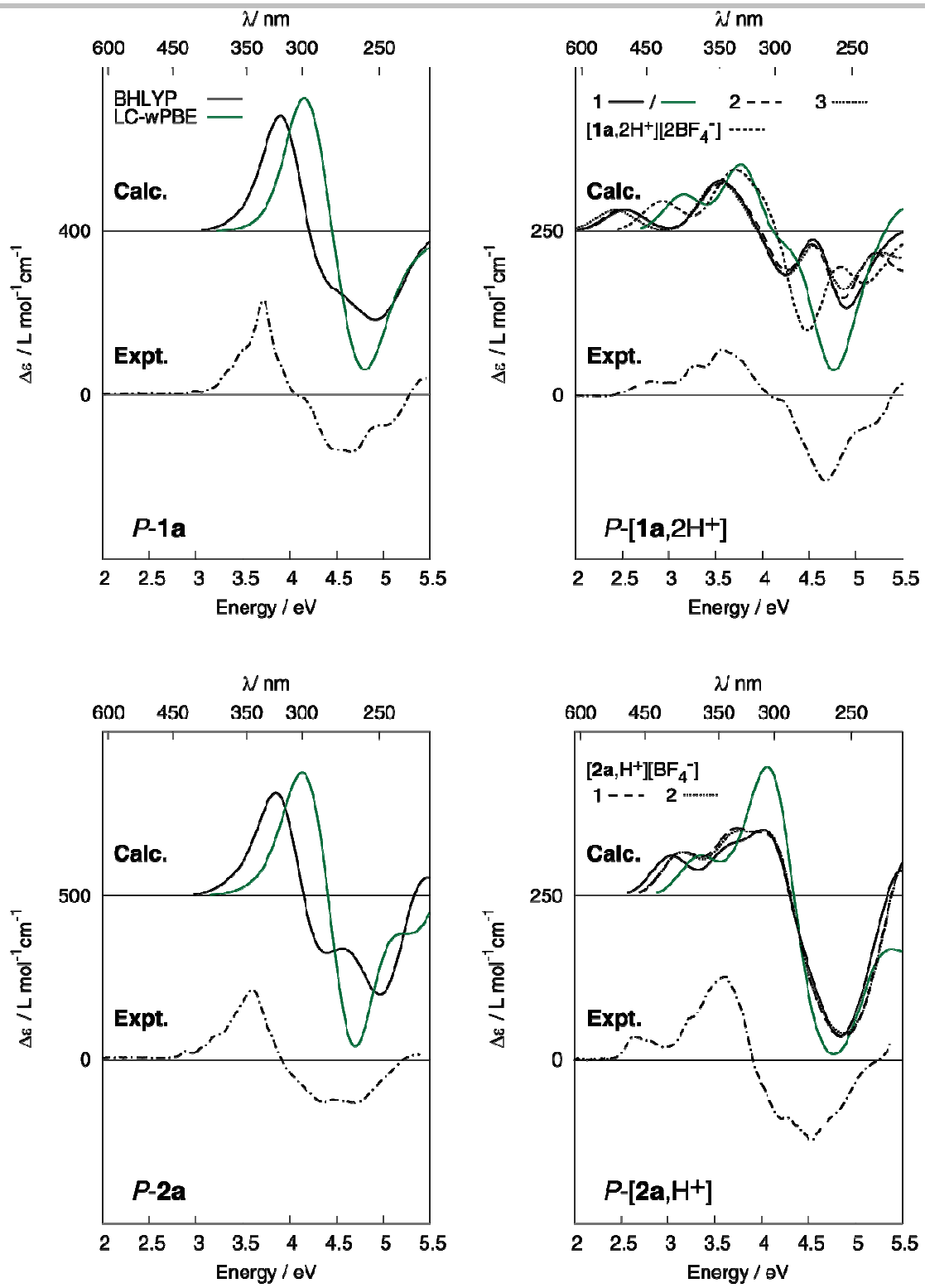

Figure S22. Comparison of experimental and calculated TDDFT CD spectra of ligand species *P*-**1a** and *P*-[**1a**,2H$^+$] (top) and cycloplatinated complexes *P*-**2a** and *P*-[**2a**,H$^+$] (bottom). No spectral shift has been applied. DCM solvent. Numbers listed (1, 2, 3) correspond to different conformers examined (compare Figure S20 in the case of [**1a**,2H$^+$] and Figure S21 in the case of [**2a**,H$^+$][BF$_4^-$]).

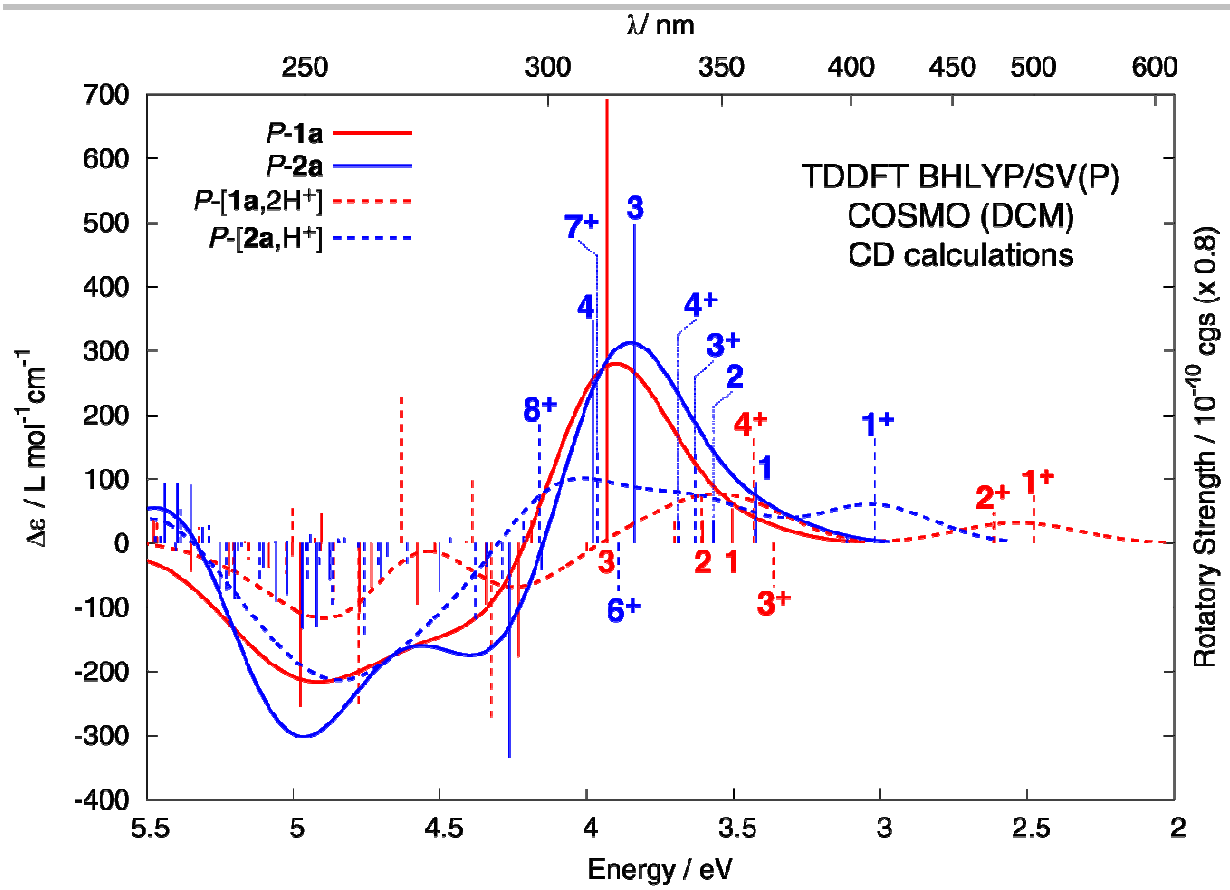

Figure S23. Comparison of the calculated BHLYP CD spectra of ligand species *P*-**1a** (red solid line) and *P*-[**1a**,2H$^+$]-1 (red dashed line) and cycloplatinated complexes *P*-**2a** (blue solid line) and *P*-[**2a**,H$^+$] (blue dashed line). No spectral shifts have been applied. Numbered excitations correspond to those analyzed in detail.

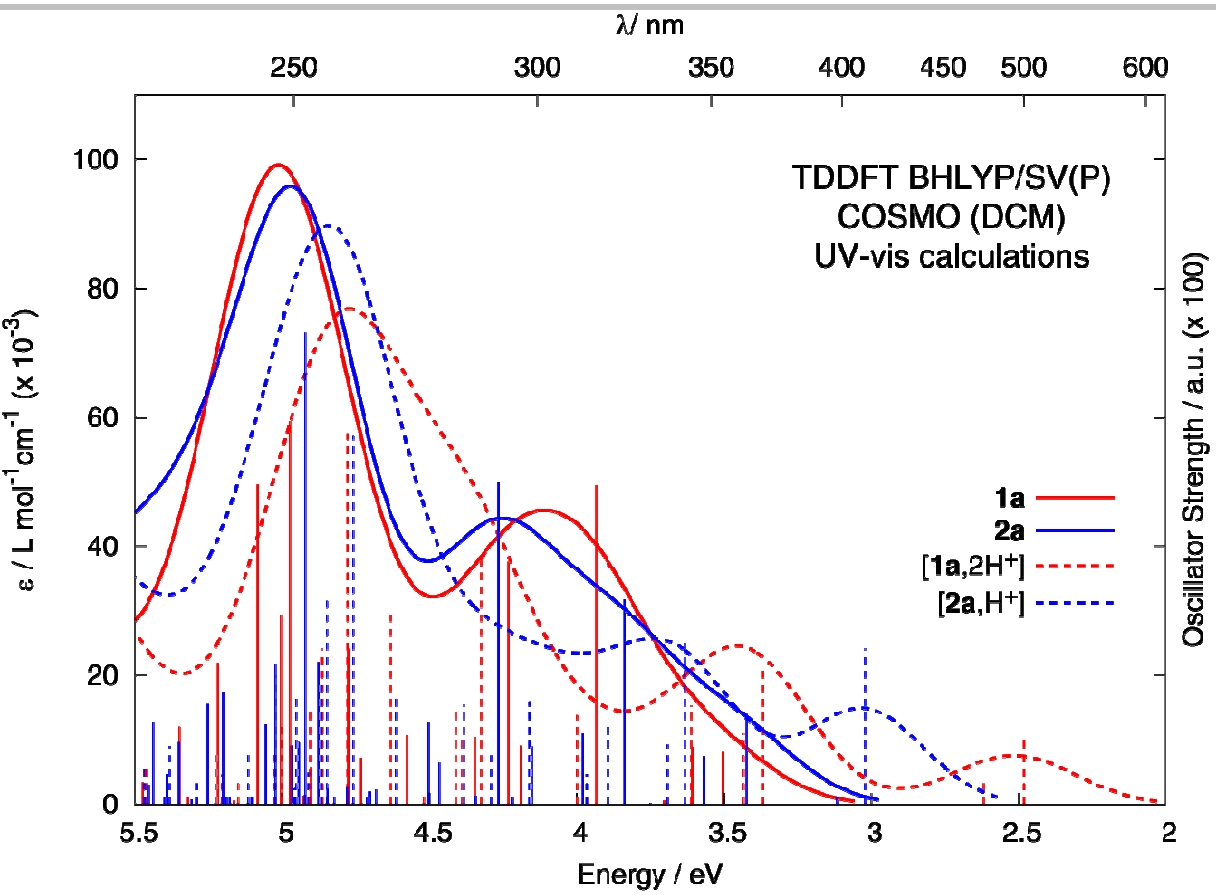

Figure S24. Comparison of the calculated BHLYP UV-vis spectra of ligand species *P*-**1a** (red solid line) and *P*-[**1a**,2H$^+$]-1 (red dashed line) and cycloplatinated complexes *P*-**2a** (blue solid line) and *P*-[**2a**,H$^+$] (blue dashed line). No spectral shifts have been applied.

Table S5. Selected dominant excitations and occupied (occ) – unoccupied (unocc) MO pair contributions (greater than 10%) of *P*-**1a** and *P*-[**1a**,2H$^+$]-1 ligand species. BHLYP/SV(P) DCM calculations.

Excitation	E / eV	λ / nm	f / au	R / 10^{-40} cgs	occ no.	unocc no.	%
				1a			
#1	3.50	354	0.0813	67.86	106	107	33.0
					105	107	31.1
					106	108	17.2
#2	3.61	344	0.0885	43.93	106	107	44.1
					105	107	22.5
					106	108	16.4
#3	3.93	315	0.4944	865.51	105	108	35.1
					106	108	28.1
					105	107	15.5
				[**1a**,2H$^+$]-1			
#1$^+$	2.48	500	0.1000	92.13	106	107	91.7
#2$^+$	2.62	474	0.0392	60.23	105	107	85.7
#3$^+$	3.37	368	0.2177	-83.96	104	107	76.6
#4$^+$	3.43	361	0.1105	211.81	106	108	52.9
					106	109	18.7

Table S6. Selected dominant excitations and occupied (occ) – unoccupied (unocc) MO pair contributions (greater than 10%) of *P*-**2a** and *P*-[**2a**,H^+] cycloplatinated species. BHLYP/SV(P) DCM calculations.

Excitation	*E* / eV	λ / nm	*f* / au	*R* / 10^{-40} cgs	occ no.	unocc no.	%
			2a				
#1	3.42	362	0.1397	118.97	140	141	53.8
					139	141	17.4
					140	142	10.0
#2	3.57	347	0.0751	44.19	139	141	39.2
					140	141	23.2
					140	142	17.4
#3	3.84	323	0.3178	624.08	139	142	52.9
					138	141	10.3
#4	3.98	311	0.1107	434.60	139	142	27.3
					138	141	21.8
					140	142	10.9
			[**2a**,H^+]				
#1$^+$	3.02	410	0.2411	209.98	140	141	75.5
					139	141	10.2
#3$^+$	3.63	341	0.2541	173.11	138	141	45.9
					140	142	26.3
#4$^+$	3.69	336	0.0923	53.93	138	141	28.7
					139	142	22.7
					140	142	20.5
#6$^+$	3.89	319	0.1209	-91.83	139	142	23.8
					140	142	19.9
					140	143	16.8
					136	141	15.9
#7$^+$	3.97	313	0.0467	176.29	136	141	47.5
					139	142	14.4
					139	143	13.5
#8$^+$	4.16	298	0.1597	231.63	140	143	50.7
					139	142	15.6

Table S7. Calculated S_0 frontier molecular orbitals energies and HOMO-LUMO gaps (ΔE), in eV, at $S_0^{\{DFT\}}$, $S_1^{\{TDDFT\}}$, and $T_1^{\{TDDFT\}}$ geometries calculated with BHLYP/SV(P) DCM. [a]

	HOMO	LUMO	ΔE
		$S_0^{\{DFT\}}$	
P-**1a**	-6.66	-1.25	5.41
P-[**1a**,2H$^+$]-1	-7.67	-3.82	3.85
P-**2a**	-6.53	-1.22	5.31
P-[**2a**,H$^+$]	-7.17	-2.62	4.54
		$S_1^{\{TDDFT\}}$	
P-**1a**	-6.31	-1.45	4.86
P-[**1a**,2H$^+$]-1	-7.48	-4.19	3.30
P-[**1a**,2H$^+$]-2	-7.48	-4.19	3.29
P-**2a**	-6.22	-1.43	4.80
P-[**2a**,H$^+$]	-6.96	-2.77	4.18
		$T_1^{\{TDDFT\}}$	
P-**1a**	-6.38	-1.38	5.00
P-[**1a**,2H$^+$]-1	-7.52	-4.17	3.35
P-[**1a**,2H$^+$]-2	-7.53	-4.16	3.36
P-**2a**	-6.27	-1.35	4.92
P-[**2a**,H$^+$]	-6.99	-2.70	4.29

[a] The corresponding acetone data appeared to be very similar and therefore they are not shown.

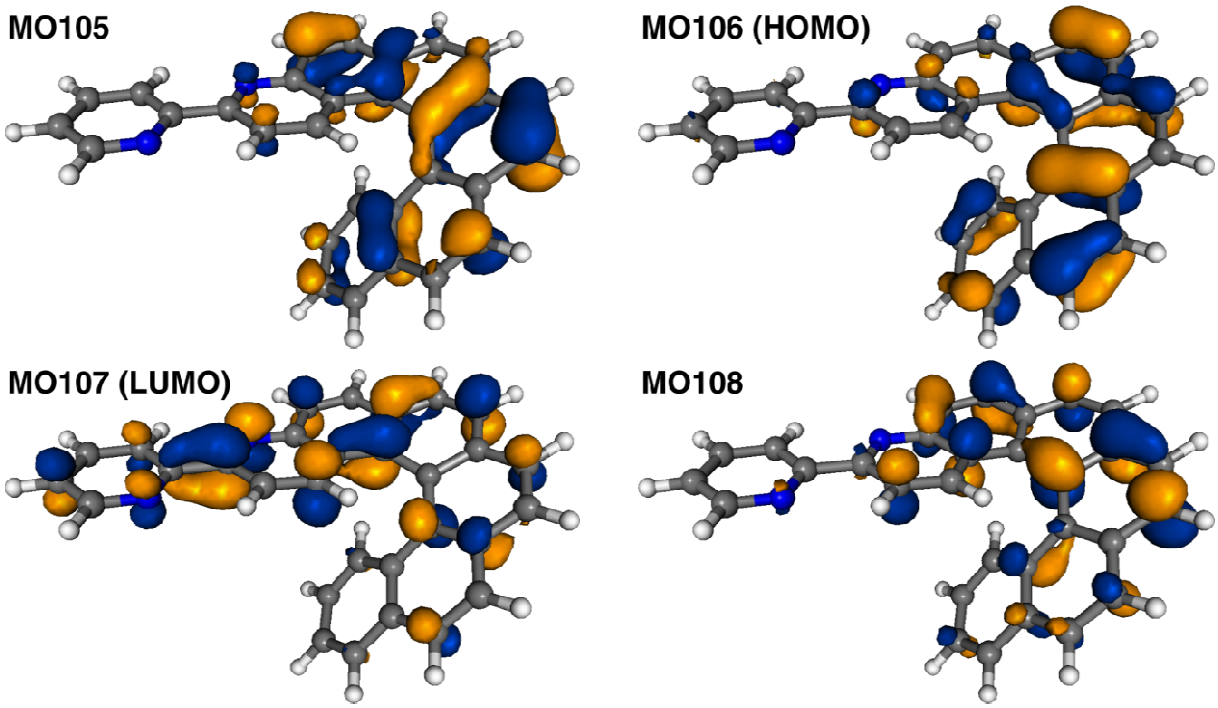

Figure S25. Isosurfaces (0.04 au) of selected MOs of **1a**.

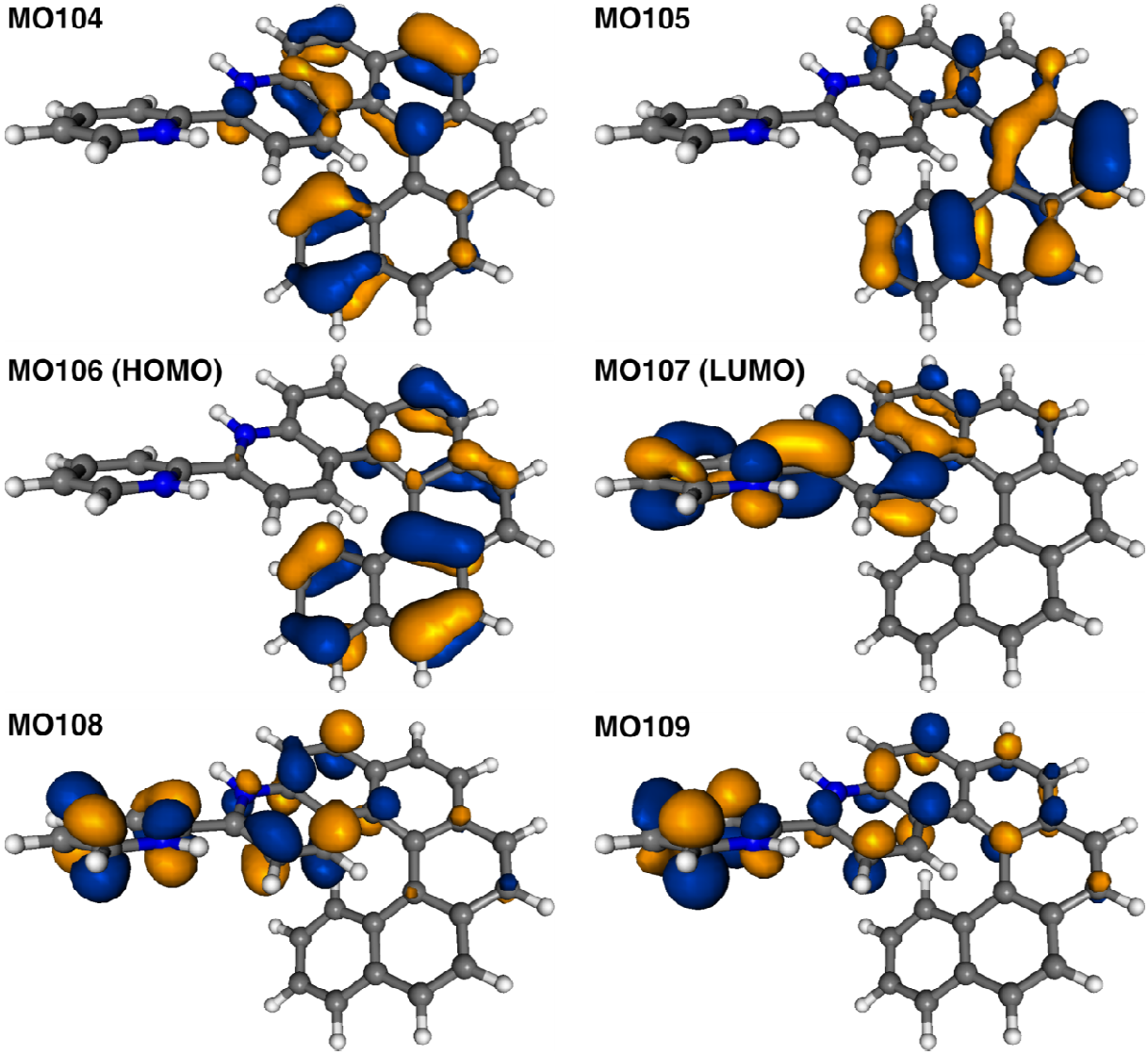

Figure S26. Isosurfaces (0.04 au) of selected MOs of [**1a**,$2H^+$]-1.

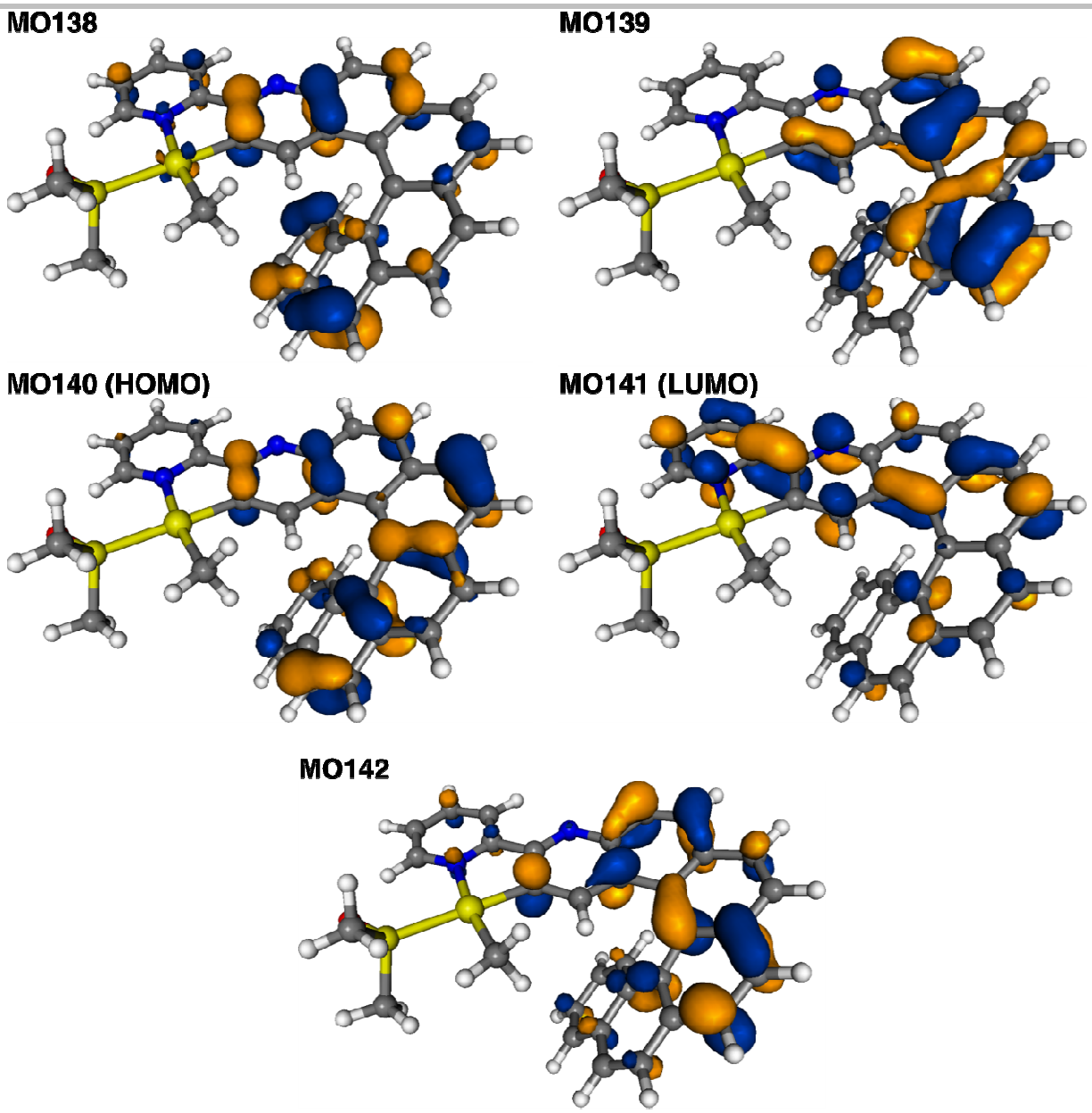

Figure S27. Isosurfaces (0.04 au) of selected MOs of **2a**.

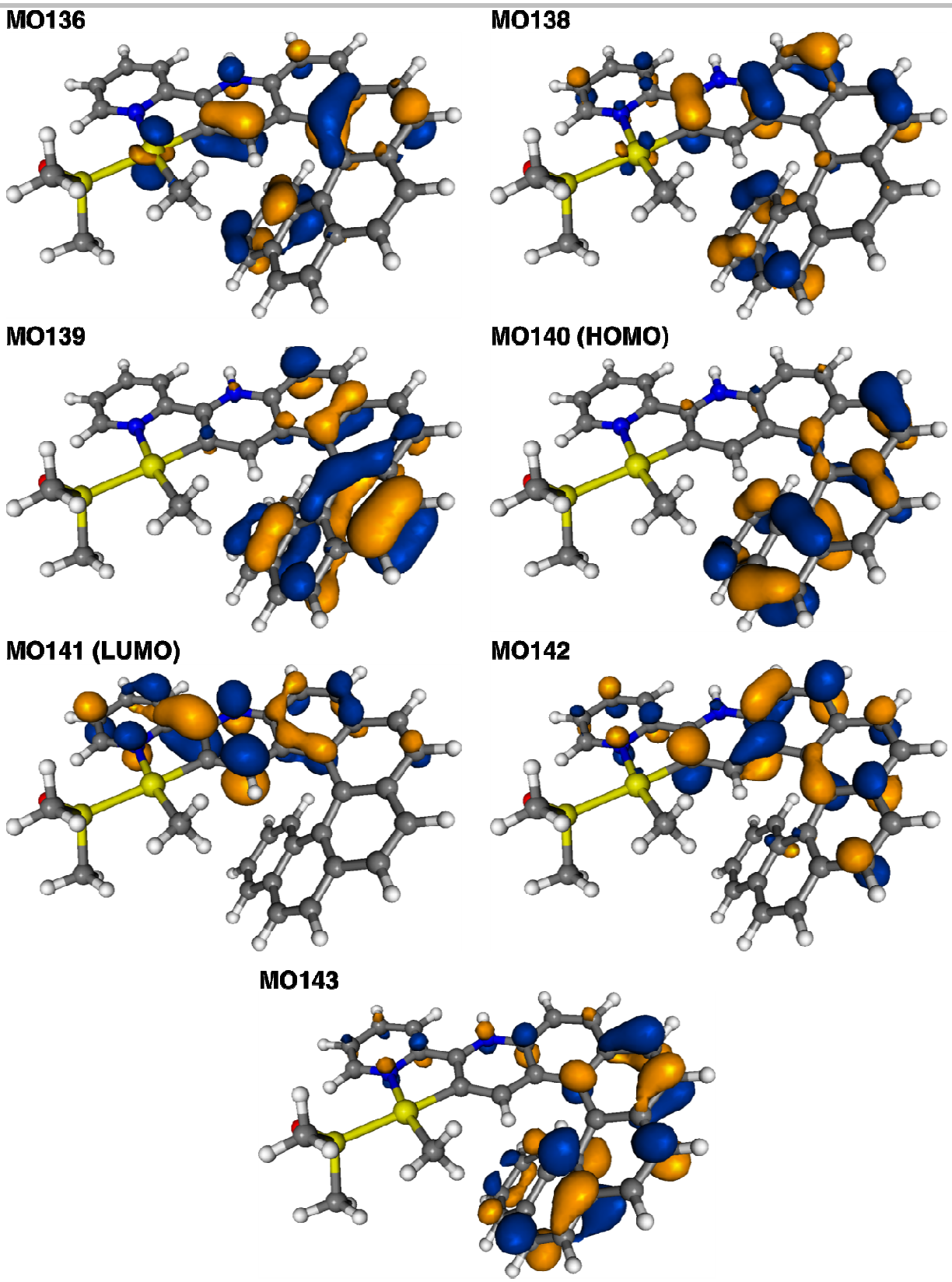

Figure S28. Isosurfaces (0.04 au) of selected MOs of [**2a**,H^+].

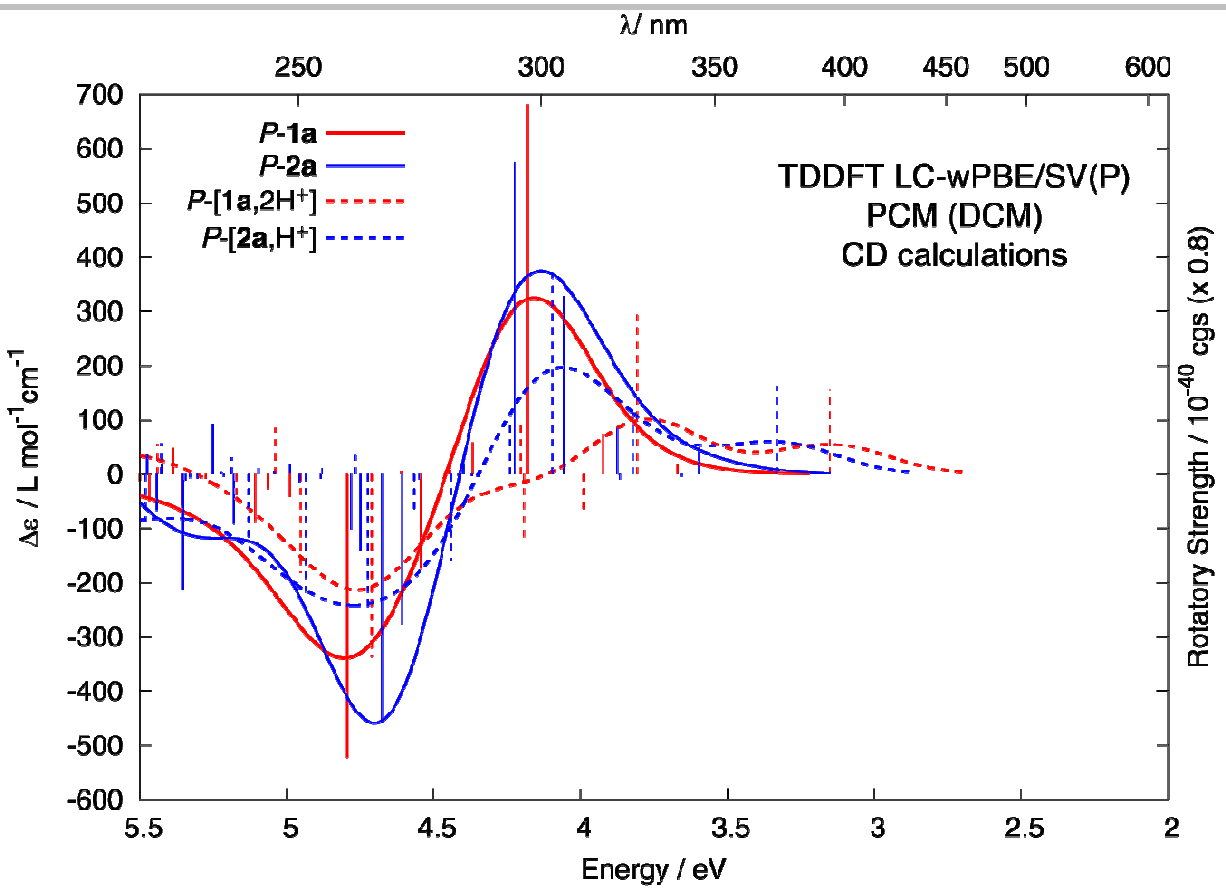

Figure S29. Comparison of the calculated LC-wPBE CD spectra of ligand species *P*-**1a** (red solid line) and *P*-[**1a**,2H$^+$]-1 (red dashed line) and cycloplatinated complexes *P*-**2a** (blue solid line) and *P*-[**2a**,H$^+$] (blue dashed line). No spectral shifts have been applied.

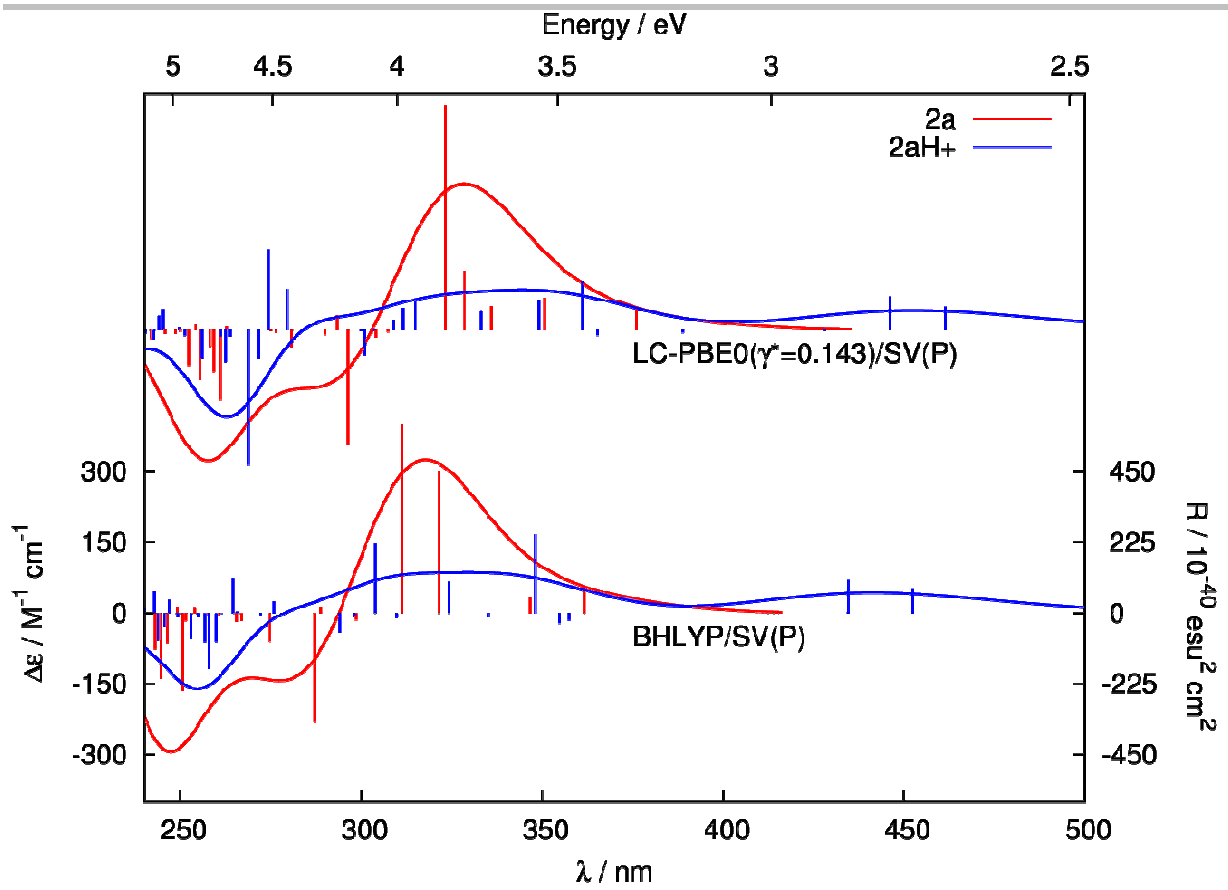

Figure S30. Comparison of calculated spectra of standard hybrid functional (BHLYP) and tuned range-separated hybrid functional (LC-PBE0*) for *P*-**2a** (2a) and *P*-[**2a**,H^+] (2aH+) in the gas phase.

Table S8. Experimental and calculated emission data of ligand species **1a** and [**1a**,$2H^+$] and of cycloplatinated complexes **2a** and [**2a**,H^+]. Energies, in eV.

	P-**1a**	*P*-[**1a**,$2H^+$]-# [a]		*P*-**2a**	*P*-[**2a**,H^+]
		1	2		
Expt. [b]					
298 K	2.94, 2.79, 2.62	2.10		2.27, 2.12	2.23, 2.10
77 K	F: 2.97, 2.81, 2.63 P: 2.33, 2.15, 1.99	F: 3.13, 2.98, 2.81, 2.63 [g] P: 2.34, 2.15, 2.00 [g]		2.31, 2.13, 1.95	2.29, 2.10, 1.94 [g]
Calc. BHLYP/SV(P) [c]					
S_1 {TDDFT} [d]	2.99 (0.4642/427.88)	1.86 (0.1631/174.24)	1.87 (0.1741/194.33)	2.94 (0.5507/459.99)	2.66 (0.3444/268.69)
T_1 {TDDFT} [e]	2.18	1.49	1.50	2.16	2.08
T_1 {DFT} [f]	2.08	1.60	1.61	2.06	2.08

[a] Conformer #1: dihedral angle N-C-C'-N' of -150.0°, -170.5°, -175.7°, and -170.9° for S_0 ground state, S_1 excited state, T_1 excited state, and triplet configuration, respectively. Conformer #2: dihedral angle N-C-C'-N' of 151.0°, 171.5°, 172.2°, and 168.7° for S_0 ground state, S_1 excited state, T_1 excited state, and triplet configuration, respectively. [b] 298 K: DCM / acetone data for ligand / cycloplatinated species, 77 K: recorded in diethyl ether / isopentane / ethanol. F = fluorescence. P = phosphorescence. [c] DCM /acetone calculations for ligand / cycloplatinated species. [d] TDDFT S_1-S_0 energy difference at TDDFT BHLYP/SV(P) optimized S_1 geometry. In parentheses oscillator strength / rotatory strength values in 10^{-40} cgs are listed. To convert to integrated CPL intensity, in cgs units of power output per molecule, the following expression can be used: $\Delta I = 1.60041320 \cdot 10^{37} \cdot R_{cgs} \cdot E_{cgs}^4$. [e] TDDFT T_1-S_0 energy difference at TDDFT BHLYP/SV(P) optimized T_1 geometry. [f] TDDFT T_1-S_0 energy difference at DFT BP/SV(P) optimized triplet configuration. [g] At 77K, the equilibrium $B+H^+ \rightleftarrows BH^+$ is frozen.

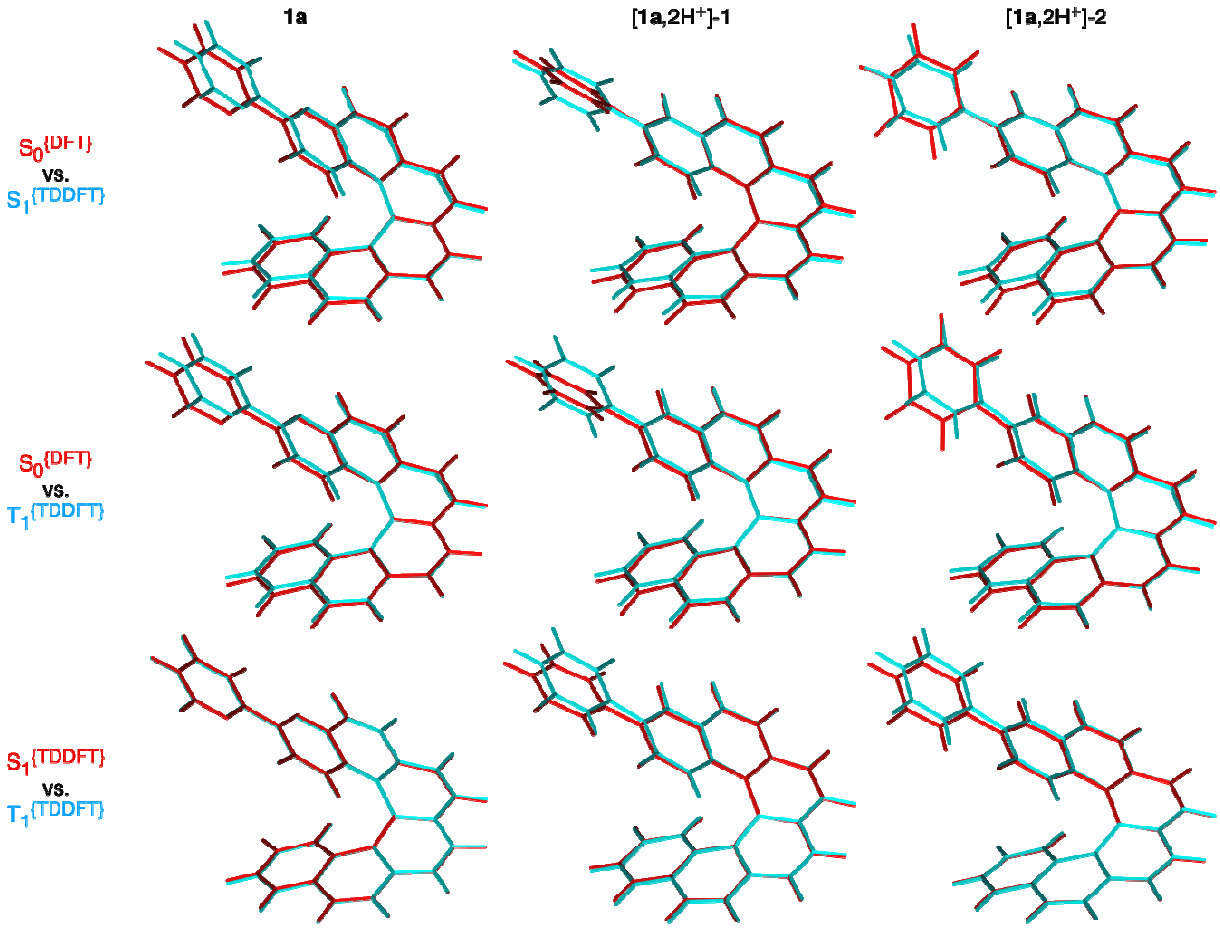

Figure S31. Overlays of optimized ground-state, $S_0^{\{DFT\}}$ (BP/SV(P) DCM), and excited-states, $S_1^{\{TDDFT\}}$ and $T_1^{\{TDDFT\}}$ (BHLYP/SV(P) DCM), structures of the ligand species.

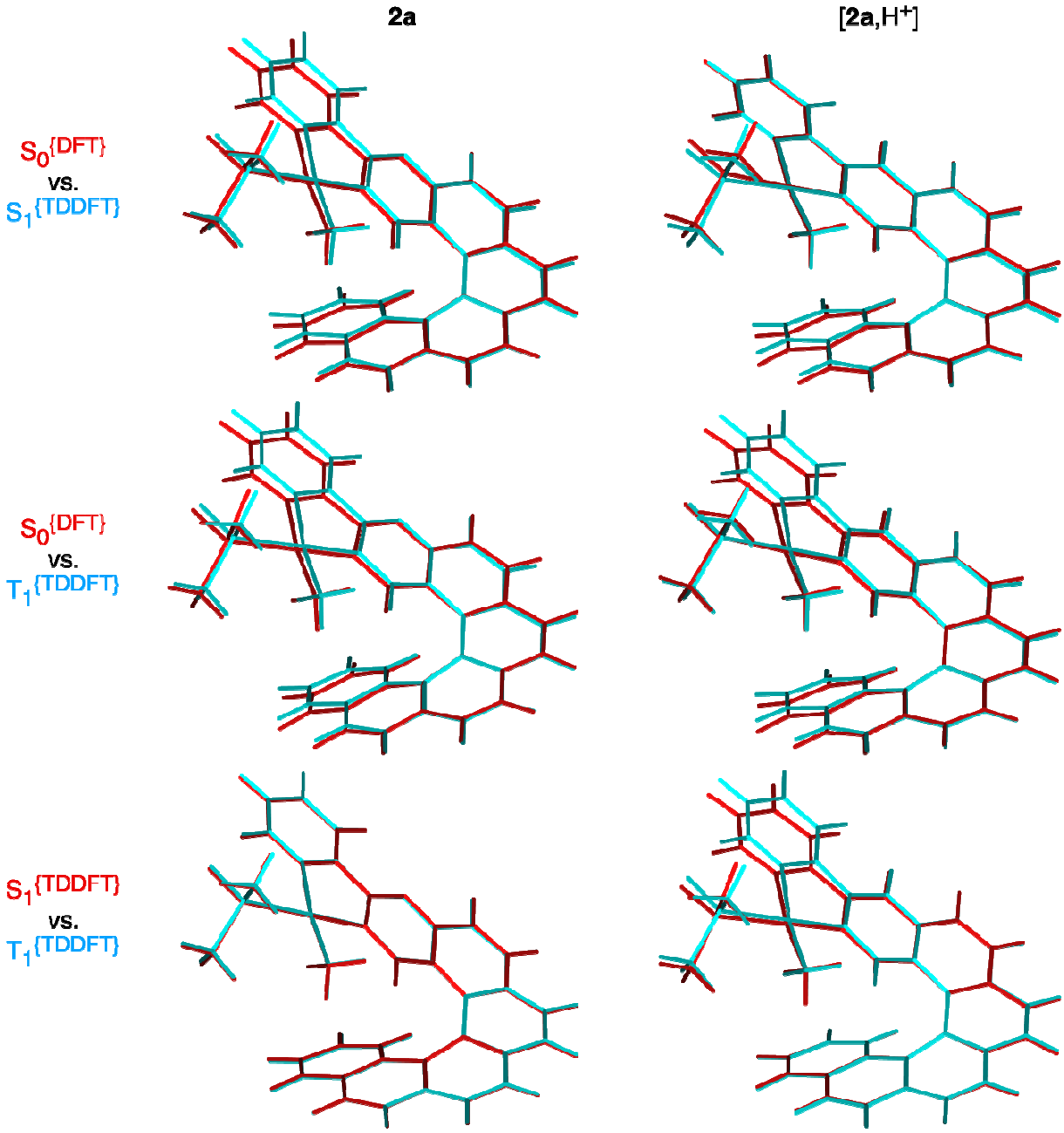

Figure S32. Overlays of optimized ground-state, $S_0^{\{DFT\}}$ (BP/SV(P) acetone), and excited-states, $S_1^{\{TDDFT\}}$ and $T_1^{\{TDDFT\}}$ (BHLYP/SV(P) acetone), structures of the metal-complex species.

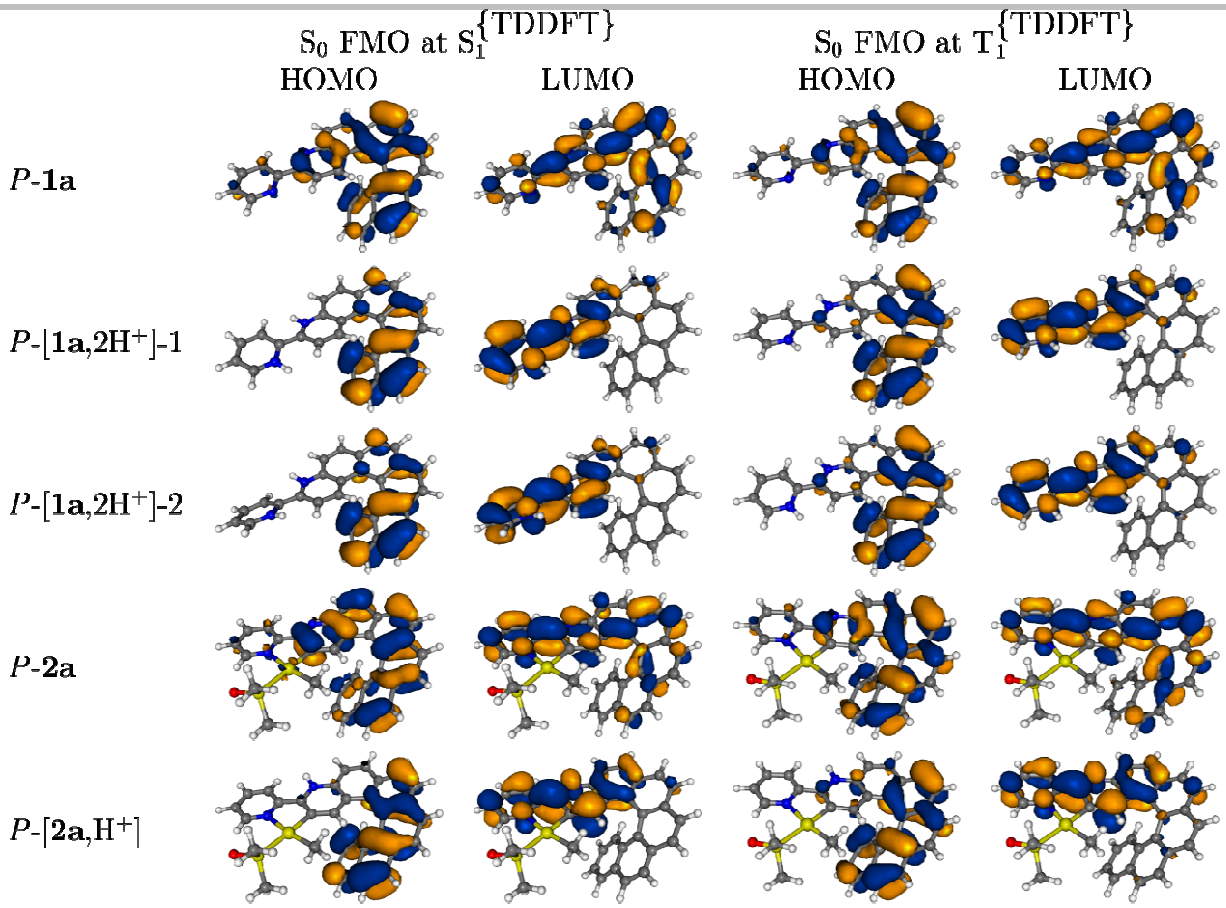

Figure S33. Isosurfaces (0.03 au) of frontier molecular orbitals (FMOs) of S0 at the $S_1^{\{TDDFT\}}$ and $T_1^{\{TDDFT\}}$ excited-state geometry calculated with BHLYP/SV(P) DCM. The corresponding acetone data appeared to be very similar and therefore they are not shown.

Table S9. HOMO-to-LUMO character (in %) of S_0-S_1 absorption along with S_1-S_0 and T_1-S_0 emission transitions for ligand species **1a** and [**1a**,$2H^+$] and of cycloplatinated complexes **2a** and [**2a**,H^+]. BHLYP/SV(P) solvent data.

	S_0-S_1	S_1-S_0	T_1-S_0
P-**1a**	33.0	93.7	72.3
P-[**1a**,$2H^+$]-1	91.7	96.5	76.0
P-[**1a**,$2H^+$]-2	---	96.4	75.9
P-**2a**	53.8	92.3	68.9
P-[**2a**,H^+]	75.5	90.1	61.6

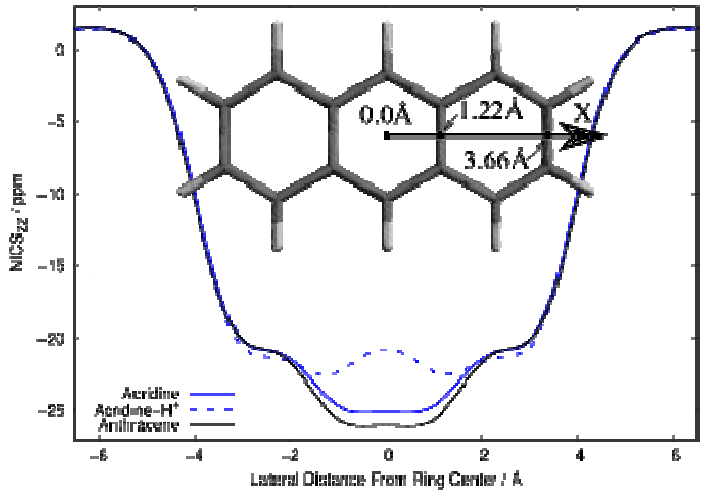

Figure S34. A model to rationalize the breaking of π-conjugation upon protonation for complex **2a**. The nuclear-independent chemical shift (NICS) is used to investigate the extent of aromaticity in a poly-aromatic conjugated system. $NICS_{ZZ}$-X scans are plotted, along with the anthracene molecular structure highlighting the lateral distance measurement. The *acridine* structure replaces the CH group in position 10 (top center) with a nitrogen to give a planar fragment similar to what is found in the ligand of **2a**. Acridine can be subsequently protonated to form acridine-H^+. $NICS_{ZZ}$-X scans were calculated at 1.7Å above the molecular plane, as suggested in Reference 46. The flat $NICS_{ZZ}$ values in the ring centers of anthracene and acridine suggest global ring currents. However, upon protonation the center ring's curve is no longer flat suggesting a significant loss of aromaticity.

Atomic coordinates

The optimized BP/SV(P) COSMO DCM geometries of ligand species **1a** and [**1a**,$2H^+$]-1 and of cycloplatinated complexes **2a** and [**2a**,H^+] (the atomic symbol followed by three Cartesian coordinates, in Å) with the corresponding total energy values in solution *E* (in au, listed as 'Total energy + OC corr.' in output files).

P-**1a**

E = -1262.727515

C	3.6062020	-3.8139641	-0.5411308
C	2.6162200	-3.0834399	-1.2375152
N	2.1319701	-3.4848062	-2.4360812
C	2.6162106	-4.6165376	-2.9713420
C	3.6003285	-5.4111363	-2.3546315
C	4.1028631	-4.9942527	-1.1098396
C	2.0619066	-1.8196377	-0.6660464
N	2.5291534	-1.4186085	0.5202497
C	2.0416784	-0.2794830	1.0817833
C	0.9766891	0.4959315	0.4914267
C	0.5556935	0.0745100	-0.8026101
C	1.0930523	-1.0639466	-1.3859186
C	2.6700547	0.1815495	2.2896392
C	2.3334157	1.4069645	2.8137278
C	1.2846305	2.2082052	2.2403755
C	0.4830722	1.6908997	1.1674634
C	1.0887952	3.5489997	2.7029949
C	0.1993971	4.3797934	2.0558471
C	-0.6886844	3.8634144	1.0577382
C	-0.6858873	2.4561308	0.7452290
C	-1.8447654	1.9307657	0.0312574
C	-2.6367327	2.8510804	-0.7344438
C	-2.4536777	4.2632562	-0.5783286
C	-1.5794168	4.7488697	0.3695612
C	-3.6599225	2.3637593	-1.6196850
C	-3.9742000	1.0261127	-1.6773533
C	-3.3659876	0.0996039	-0.7637053
C	-2.3300433	0.5537473	0.1328544
C	-3.8282065	-1.2467773	-0.6886526
C	-3.3457866	-2.1201545	0.2809285
C	-2.3958213	-1.6541565	1.2239580
C	-1.8999601	-0.3544406	1.1445617
H	0.7913607	-1.3949470	-2.3900320
H	-2.0499098	-2.3194186	2.0323026
H	-3.7206224	-3.1555103	0.3357083
H	-1.5238735	5.8280938	0.5880768
H	-4.6038292	-1.5759488	-1.4003980
H	-3.0826225	4.9487672	-1.1700001
H	-4.7468078	0.6588356	-2.3731619
H	-4.1959108	3.0940367	-2.2485832
H	-1.1831096	-0.0144516	1.9048155
H	0.1335477	5.4489651	2.3174920
H	1.7191852	3.9259504	3.5250830
H	3.4644160	-0.4433171	2.7269830
H	2.8755931	1.8092970	3.6858952
H	-0.1767839	0.6720198	-1.3633235
H	2.1972202	-4.9116389	-3.9518359
H	3.9608048	-6.3313595	-2.8416701
H	4.8754661	-5.5834052	-0.5884537

H	3.9636350	-3.4382209	0.4287899

P-**2a**

E = -1974.573378

Pt	-0.5747156	-0.5548722	3.8887759
O	0.6630562	0.0494855	7.0237674
C	3.3361181	-0.4585048	1.9395308
N	1.1969166	-1.0179740	0.0804242
C	-2.6316681	-0.8415939	3.8527364
S	-0.6266992	-0.2677056	6.2739295
C	4.3037361	-0.1875697	2.9159226
H	5.3708564	-0.1296850	2.6452013
C	3.8869481	0.0090906	4.2444513
H	4.6083352	0.2262572	5.0476887
C	2.5200748	-0.0755643	4.5491949
H	2.1341167	0.0599461	5.5756616
N	1.5874011	-0.3350008	3.6056299
C	1.9809131	-0.5228072	2.3109912
C	0.8839825	-0.7770359	1.3544650
C	-0.4568593	-0.7624084	1.8781977
C	-1.4759097	-0.8778808	0.9290574
C	-1.1964161	-1.0555844	-0.4568715
C	-2.2249041	-1.2059038	-1.4830147
C	-3.6351369	-0.8861218	-1.2913041
C	-4.1684065	0.1174650	-0.3760663
C	-3.4537649	1.3252338	0.0401861
C	-2.2767910	1.8003466	-0.6094821
H	-1.8802962	1.2521805	-1.4754274
C	-1.6354370	2.9691515	-0.2050508
H	-0.7369569	3.3104889	-0.7455538
C	-2.1348761	3.7230437	0.8862942
H	-1.6129661	4.6372596	1.2147564
C	-3.3099204	3.3191948	1.5120223
H	-3.7417194	3.9204461	2.3303053
C	-4.0058112	2.1494446	1.0885928
C	-5.2898497	1.8280535	1.6460856
H	-5.6867280	2.4527109	2.4640280
C	-6.0472070	0.8165388	1.1032847
H	-7.0745921	0.6317919	1.4595024
C	-5.5312772	-0.0194507	0.0533073
C	-6.4040452	-0.9479758	-0.6017271
H	-7.4500276	-1.0240175	-0.2608056
C	-5.9675169	-1.6529287	-1.7027390
H	-6.6651970	-2.2722865	-2.2908116
C	-4.5860430	-1.6293574	-2.0799554
C	-4.1504957	-2.3430138	-3.2430882
H	-4.9067298	-2.8563082	-3.8602399
C	-2.8203394	-2.3502733	-3.6062947
H	-2.4928704	-2.8310751	-4.5430869
C	-1.8289415	-1.8245093	-2.7166607
C	-0.4341093	-1.9727181	-3.0393773
H	-0.1703082	-2.3845795	-4.0278801
C	0.5490333	-1.6208268	-2.1441761
H	1.6200582	-1.7117247	-2.3853302
C	0.1929448	-1.2060544	-0.8156394
H	-3.1098478	0.0006741	3.2999801
H	-3.1174913	-0.9026943	4.8538924
H	-2.8720252	-1.7883994	3.3155354
C	-1.3582162	-1.7162770	7.1127623
H	-1.4187320	-1.4759761	8.1948762

H	-0.6535306	-2.5537251	6.9339551
H	-2.3550331	-1.9449659	6.6832959
C	-1.8218598	1.0278335	6.7526737
H	-2.8186449	0.8086271	6.3185679
H	-1.4159627	1.9752194	6.3434835
H	-1.8500979	1.0580476	7.8619748
H	-2.5262806	-0.8658343	1.2517065
H	3.5930132	-0.6229504	0.8822333

P-[**1a**,2H$^+$]-1

E = -1263.564325

N	-3.7038993	-1.1142510	-2.8581389
C	-3.6351172	-1.1247343	-1.4918229
C	-2.3007204	-1.1054351	-0.8687475
C	-1.1703038	-0.4974064	-1.4406383
C	-4.8649540	-1.1043124	-3.5527410
C	-6.0812071	-1.1114943	-2.8694439
C	-6.0648336	-1.1280135	-1.4645348
C	-4.8414298	-1.1311373	-0.7741758
H	-2.8271702	-1.1458095	-3.3984159
H	-4.7752843	-1.1013109	-4.6484321
H	-7.0227752	-1.1053906	-3.4374178
H	-7.0085919	-1.1256344	-0.8974165
H	-4.8312074	-1.1012996	0.3252550
C	0.0382938	-0.4797481	-0.7391493
C	0.1717699	-1.0594101	0.5477855
C	-0.9835717	-1.7601068	1.0549491
N	-2.1525560	-1.7132896	0.3380720
C	-0.9264896	-2.5448978	2.2376686
C	0.3035190	-2.7209755	2.8352520
C	1.4891938	-2.0624741	2.3626223
C	1.4064452	-1.0814621	1.3138603
C	2.5868963	-0.2929182	0.9922929
C	2.7564043	-2.4264062	2.9071772
C	3.9099155	-1.9101256	2.3491830
C	3.8561897	-0.8633369	1.3770351
C	5.0675354	-0.3758962	0.7901750
C	5.0281843	0.6452303	-0.1333393
C	3.8145457	1.3728582	-0.3626791
C	2.6033392	0.9921750	0.3078877
C	1.5146903	1.9699710	0.3408381
C	1.5713748	3.1168921	-0.5339751
C	2.7310883	3.3327707	-1.3531191
C	3.8346453	2.5213059	-1.2255722
C	0.5102505	4.0684266	-0.5259145
C	-0.5583127	3.9462714	0.3568193
C	-0.5774704	2.8712460	1.2798185
C	0.4305127	1.9080496	1.2651054
H	-1.2348228	-0.0015105	-2.4196662
H	0.9120114	-0.0205044	-1.2198236
H	-2.9459948	-2.2439394	0.7248799
H	-1.8302310	-3.0464872	2.6164009
H	0.3953275	-3.3947355	3.7024448
H	2.8009645	-3.1763389	3.7124124
H	4.8981476	-2.2770407	2.6703783
H	6.0206819	-0.8544627	1.0664513
H	5.9454293	0.9720039	-0.6494809
H	4.7617263	2.7435406	-1.7786847
H	2.7481596	4.2010478	-2.0321031
H	0.5705313	4.9280253	-1.2139884

H	-1.3637147	4.6984157	0.3640250
H	-1.3835409	2.8030882	2.0286528
H	0.4064254	1.1109776	2.0219786

P-[**2a**,H^+]

E = -1975.010644

Pt	-0.5788852	-0.5320633	3.8776582
O	0.6439256	0.0479643	6.9855311
C	3.3679938	-0.4518095	1.9670468
N	1.1474715	-1.0222698	0.0769503
C	-2.6352601	-0.7948768	3.8176704
S	-0.6547758	-0.2621200	6.2543605
C	4.3222705	-0.1875401	2.9609380
H	5.3907607	-0.1262468	2.7006271
C	3.8864983	-0.0014171	4.2806933
H	4.5967392	0.2107132	5.0945252
C	2.5131595	-0.0856701	4.5660416
H	2.1141196	0.0472604	5.5883121
N	1.5941719	-0.3378582	3.6119924
C	2.0080864	-0.5217285	2.3194466
C	0.9020257	-0.7662867	1.3851029
C	-0.4370237	-0.7427687	1.8694247
C	-1.4496741	-0.8662034	0.9038041
C	-1.1938803	-1.0465671	-0.4839417
C	-2.2315790	-1.2011761	-1.4984321
C	-3.6363630	-0.8829838	-1.2890618
C	-4.1604292	0.1161889	-0.3657874
C	-3.4447119	1.3239945	0.0462573
C	-2.2767677	1.8073918	-0.6140442
H	-1.8912851	1.2717295	-1.4932123
C	-1.6360439	2.9768289	-0.2097478
H	-0.7483483	3.3287722	-0.7609325
C	-2.1281614	3.7231435	0.8900443
H	-1.6095281	4.6400447	1.2151759
C	-3.2954663	3.3118998	1.5252494
H	-3.7234988	3.9093964	2.3477643
C	-3.9897595	2.1404956	1.1044637
C	-5.2662775	1.8107777	1.6741384
H	-5.6573846	2.4306111	2.4981071
C	-6.0254878	0.7971536	1.1377813
H	-7.0476032	0.6064637	1.5046971
C	-5.5162035	-0.0323635	0.0803497
C	-6.3905519	-0.9660484	-0.5658439
H	-7.4316019	-1.0482168	-0.2122720
C	-5.9660598	-1.6689512	-1.6722876
H	-6.6679406	-2.2909501	-2.2514905
C	-4.5894749	-1.6378446	-2.0646639
C	-4.1636781	-2.3529896	-3.2293450
H	-4.9251950	-2.8694149	-3.8365151
C	-2.8382123	-2.3610509	-3.6098799
H	-2.5206338	-2.8416200	-4.5492300
C	-1.8434988	-1.8312236	-2.7291790
C	-0.4532783	-1.9783200	-3.0624264
H	-0.1952645	-2.3906823	-4.0514498
C	0.5480977	-1.6271318	-2.1838701
H	1.6120120	-1.7279229	-2.4507621
C	0.1762364	-1.2127464	-0.8733551
H	-3.0966026	0.0488009	3.2534083
H	-3.1328006	-0.8434211	4.8120384
H	-2.8728930	-1.7451712	3.2858189

C	-1.3776500	-1.7232350	7.0697654
H	-1.4248485	-1.5016340	8.1563898
H	-0.6780226	-2.5594635	6.8675284
H	-2.3806266	-1.9395809	6.6486282
C	-1.8430280	1.0321176	6.7391737
H	-2.8454531	0.8089621	6.3209148
H	-1.4446045	1.9795748	6.3231604
H	-1.8563032	1.0630748	7.8485842
H	-2.4980009	-0.8592333	1.2325732
H	3.6961978	-0.5931681	0.9251182
H	2.1216736	-1.1201428	-0.2393003

References

(1) Turbomole V6.5., Quantum Chemistry Group, University of Karlsruhe, Germany, 2013.

(2) Becke, A. D. *Phys. Rev. A* **1988**, *38*, 3098–3100.

(3) Perdew, J. P. *Phys. Rev. B* **1986**, *33*, 8822–8824.

(4) Perdew, J. P. *Phys. Rev. B* **1986**, *34*, 7406.

(5) Weigend, F.; Ahlrichs, R. *Phys. Chem. Chem. Phys.* **2005**, *7*, 3297–3305.

(6) Andrae, D.; Häußermann, U.; Dolg, M.; Stoll, H.; Preuß, H. *Theor. Chim. Acta* **1990**, *77*, 123–141.

(7) Feller, D. *J. Comput. Chem.* **1996**, *17*, 1571–1586.

(8) Schuchardt, K. L.; Didier, B. T.; Elsethagen, T.; Sun, L.; Gurumoorthi, V.; Chase, J.; Li, J.; Windus, T. L. *J. Chem. Info. Mod. 47*, 1045–1052.

(9) Becke, A. D. *J. Chem. Phys.* **1993**, *98*, 1372–1377.

(10) Lee, C.; Yang, W.; Parr, R. G. *Phys. Rev. B* **1988**, *37*, 785–789.

(11) Gaussian 09, Revision D.01, Frisch, M. J.; Trucks, G. W.; Schlegel, H. B.; Scuseria, G. E.; Robb, M. A.; Cheeseman, J. R.; Scalmani, G.; Barone, V.; Mennucci, B.; Petersson, G. A.; Nakatsuji, H.; Caricato, M.; Li, X.; Hratchian, H. P.; Izmaylov, A. F.; Bl, D. J. *Gaussian 09, Revision D.01*; Gaussian, Inc.: Wallingford CT, 2009.

(12) Tamm, I. *J. Phys. USSR* **1945**, *9*, 449.

(13) Dancoff, S. M. *Phys. Rev.* **1950**, *78*, 382.

(14) Hirata, S.; Head-Gordon, M. *Chem. Phys. Lett.* **1999**, *314*, 291–299.

(15) Peach, M. J. G.; Williamson, M. J.; Tozer, D. J. *J. Chem. Theory Comput.* **2011**, *7*, 3578–3585.

(16) Peach, M. J. G.; Tozer, D. J. *J. Phys. Chem. A* **2012**, *116*, 9783–9789.

(17) Peach, M. J. G.; Warner, N.; Tozer, D. J. *Mol. Phys.* **2013**, *111*, 1271–1274.

(18) Vydrov, O. A.; Scuseria, G. E. *J. Chem. Phys.* **2006**, *125*, 234109.

(19) Vydrov, O. A.; Heyd, J.; Krukau, A. V; Scuseria, G. E. *J. Chem. Phys.* **2006**, *125*, 074106.

(20) Vydrov, O. A.; Scuseria, G. E.; Perdew, J. P. *J. Chem. Phys.* **2007**, *126*, 154109.

(21) Yanai, T.; Tew, D. P.; Handy, N. C. *Chem. Phys. Lett.* **2004**, *393*, 51–57.

(22) Perdew, J. P.; Burke, K.; Ernzerhof, M. *Phys. Rev. Lett.* **1996**, *77*, 3865–3868.

(23) Valiev, M.; Bylaska, E. J.; Govind, N.; Kowalski, K.; Straatsma, T. P.; Van Dam, H. J. J.; Wang, D.; Nieplocha, J.; Apra, E.; Windus, T. L.; de Jong, W. A. *Comput. Phys. Commun.* **2010**, *181*, 1477–1489.

(24) Baer, R.; Livshits, E.; Salzner, U. *Annu. Rev. Phys. Chem.* **2010**, *61*, 85–109.

(25) Kronik, L.; Stein, T.; Refaely-Abramson, S.; Baer, R. *J. Chem. Theory Comput.* **2012**, *8*, 1515–1531.

(26) Refaely-Abramson, S.; Sharifzadeh, S.; Govind, N.; Autschbach, J.; Neaton, J. B.; Baer, R.; Kronik, L. *Phys. Rev. Lett.* **2012**, *109*, 226405.

(27) Sun, H.; Autschbach, J. *ChemPhysChem* **2013**, *14*, 2450–2461.

(28) Jacquemin, D.; Moore, B.; Planchat, A.; Adamo, C.; Autschbach, J. *J. Chem. Theory Comput.* **2014**, *10*, 1677–1685.

(29) Refaely-Abramson, S.; Baer, R.; Kronik, L. *Phys. Rev. B* **2011**, *84*, 075144.

(30) Srebro, M.; Autschbach, J. *J. Chem. Theory Comput.* **2012**, *8*, 245–256.

(31) Stein, T.; Eisenberg, H.; Kronik, L.; Baer, R. *Phys. Rev. Lett.* **2010**, *105*, 266802.

(32) Moore, B.; Autschbach, J. *ChemistryOpen* **2012**, *1*, 184–194.

(33) Gledhill, J. D.; Peach, M. J. G.; Tozer, D. J. *J. Chem. Theory Comput.* **2013**, *9*, 4414–4420.

(34) Srebro, M.; Autschbach, J. *J. Phys. Chem. Lett.* **2012**, *3*, 576–581.

(35) Cohen, A. J.; Mori-Sánchez, P.; Yang, W. *Science* **2008**, *321*, 792–794.

(36) Moore, B.; Srebro, M.; Autschbach, J. *J. Chem. Theory Comput.* **2012**, *8*, 4336–4346.

(37) II, B. M.; Autschbach, J. *J. Chem. Theory Comput.* **2013**, *9*, 4991–5003.

(38) Sun, H.; Autschbach, J. *J. Chem. Theory Comput.* **2014**, *10*, 1035–1047.

(39) Nakai, Y.; Mori, T.; Sato, K.; Inoue, Y. *J. Phys. Chem. A* **2013**, *117*, 5082–5092.

(40) Klamt, A.; Schüürmann, G. *J. Chem. Soc., Perkin Trans. 2* **1993**, 799.

(41) Klamt, A. *J. Phys. Chem.* **1996**, *100*, 3349–3353.

(42) Scalmani, G.; Frisch, M. J.; Mennucci, B.; Tomasi, J.; Cammi, R.; Barone, V. *J. Chem. Phys.* **2006**, *124*, 94107.

(43) Tomasi, J.; Mennucci, B.; Cammi, R. *Chem. Rev.* **2005**, *105*, 2999–3093.

(44) Cammi, R.; Mennucci, B.; Tomasi, J. *J. Phys. Chem. A* **2000**, *104*, 5631–5637.

(45) Cossi, M.; Barone, V. *J. Chem. Phys.* **2001**, *115*, 4708–4717.

(46) Gershoni-Poranne, R.; Stanger, A. *Chem. Eur. J.* **2014**, *20*, 5673–5688.

^{1}H NMR (CD_2Cl_2, 400 MHz)

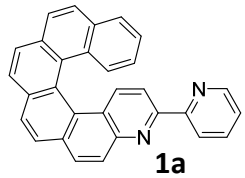

1a

^{13}C NMR (CD_2Cl_2, 101 MHz)

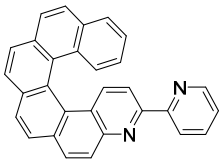

1a

^{1}H NMR (CD_2Cl_2, 400 MHz)

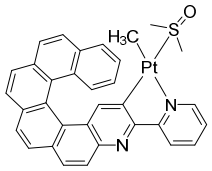

2a

^{13}C NMR (CD_2Cl_2, 101 MHz)

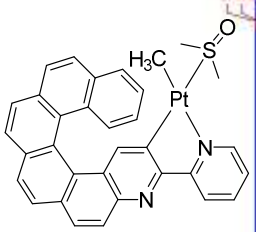

2a

^{1}H NMR ($CDCl_3$, 400 MHz)

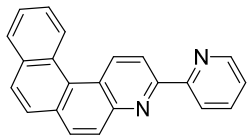

1b

^{13}C NMR (CD_2Cl_2, 75 MHz)

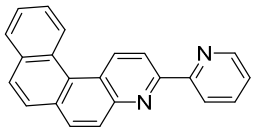

1b

^{1}H NMR (CD_2Cl_2, 400 MHz)

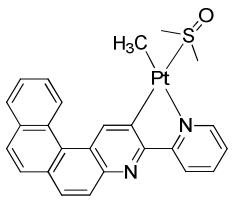

2b

^{13}C NMR (CD_2Cl_2, 101 MHz)

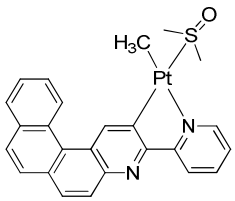

2b

^{1}H NMR (CD_2Cl_2, 400 MHz)

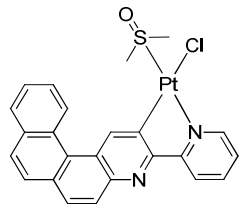

Pt(1b-H**)dmsoCl**

^{1}H NMR (CD_2Cl_2, 400 MHz)

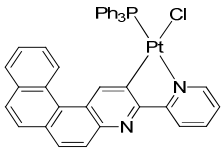

3b

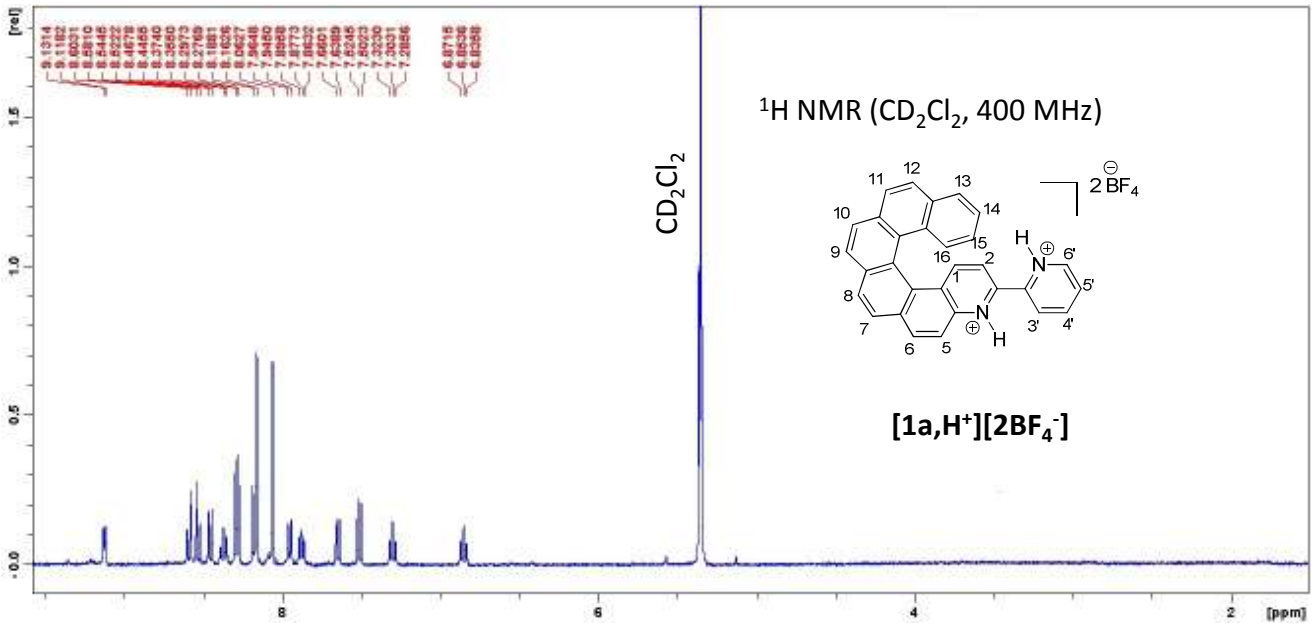
^{1}H NMR (CD_2Cl_2, 400 MHz)
CD_2Cl_2
2 BF_4^-
[1a,H$^+$][2BF_4^-]
[rel]
[ppm]

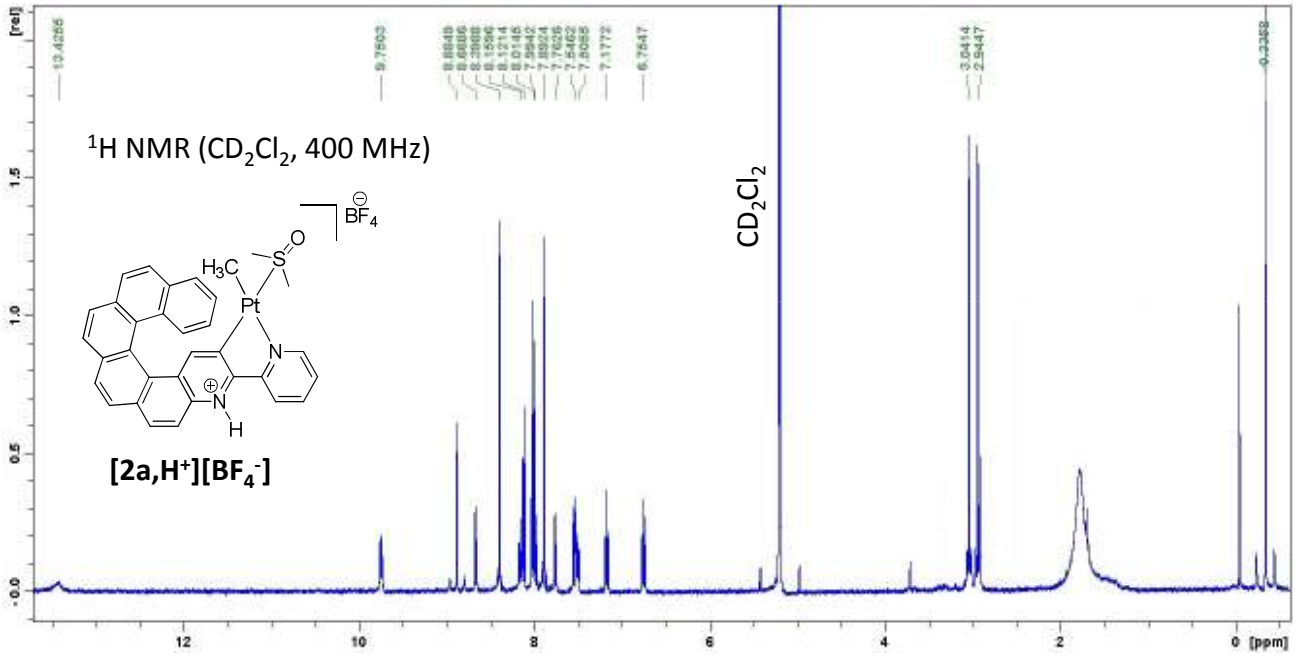
^{1}H NMR (CD_2Cl_2, 400 MHz)
CD_2Cl_2
BF_4^-
[2a,H$^+$][BF_4^-]
[rel]
[ppm]

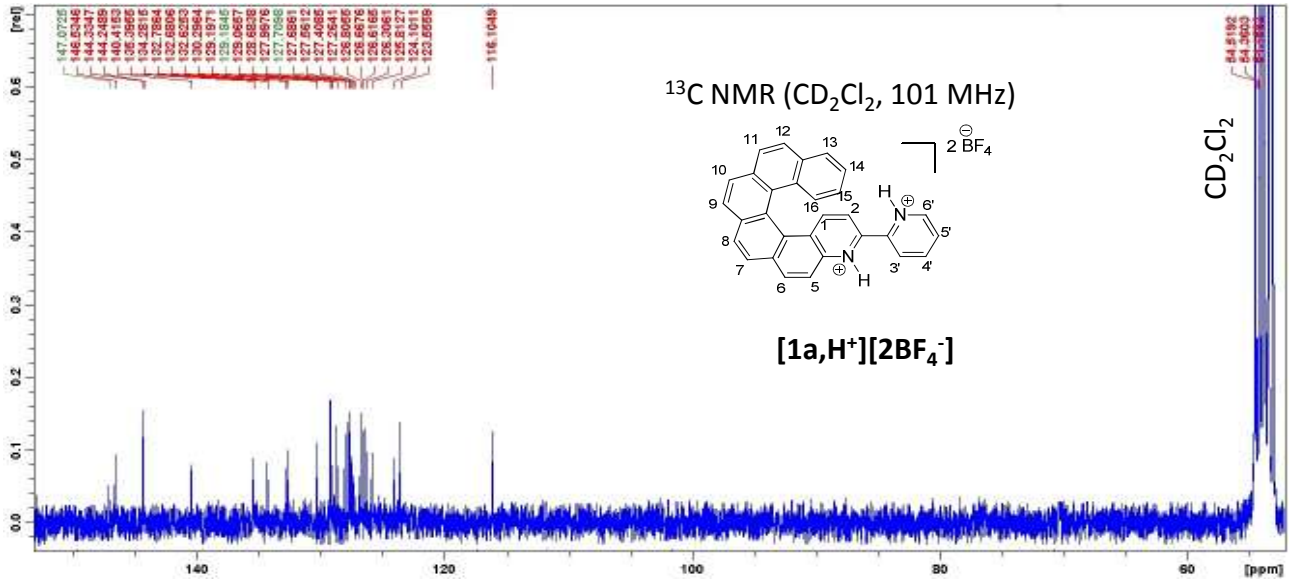
^{13}C NMR (CD_2Cl_2, 101 MHz)
CD_2Cl_2
2 BF_4^-
[1a,H$^+$][2BF_4^-]
[rel]
[ppm]

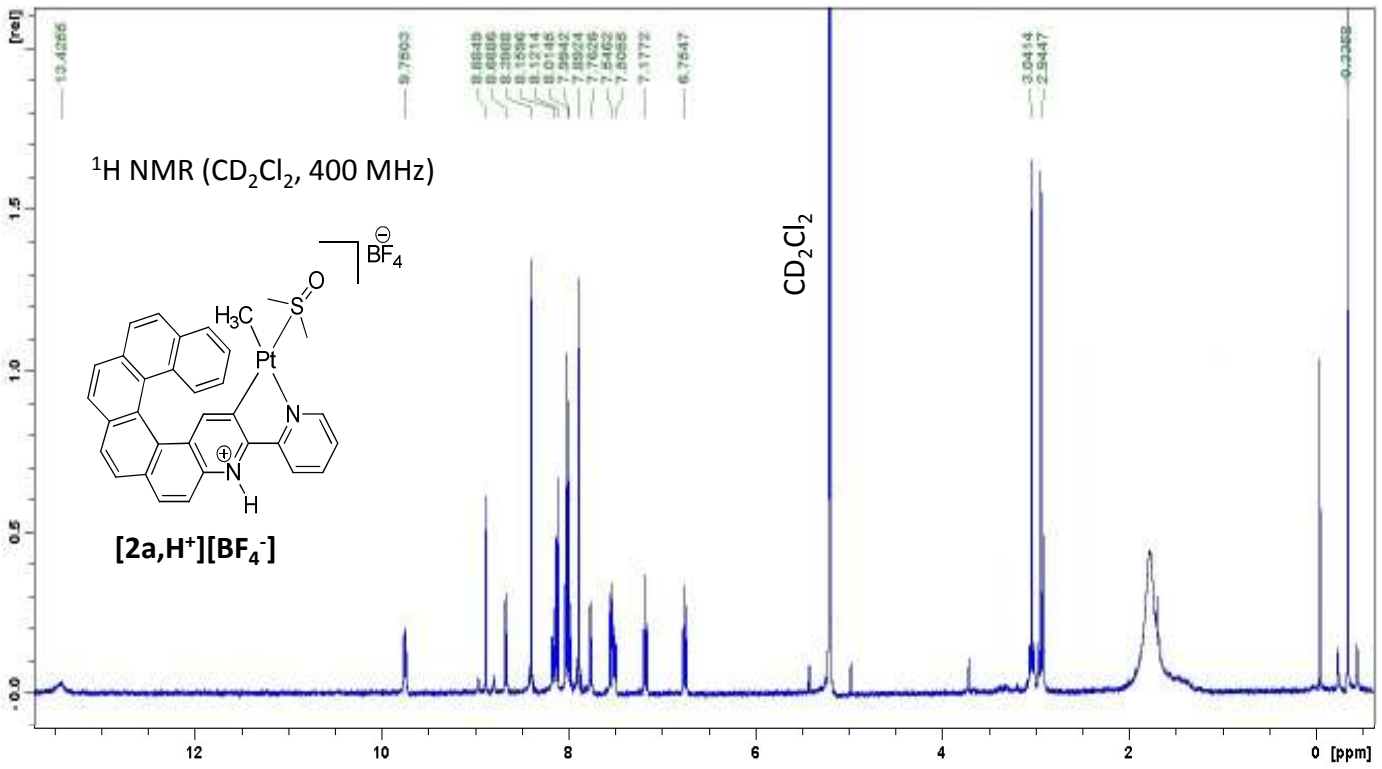
[rel]
13.4265
9.7503
8.8649
8.6886
8.3988
8.1596
8.1214
8.0145
7.9942
7.8924
7.7626
7.5462
7.5055
7.1772
6.7547
3.0414
2.9447
0.3368
1H NMR (CD2Cl2, 400 MHz)
BF4
H3C
S
O
Pt
N
N
H
[2a,H+][BF4-]
CD2Cl2
1.5
1.0
0.5
0.0
12
10
8
6
4
2
0 [ppm]